

Modeling scattering matrix containing evanescent modes for wavefront shaping applications in disordered media

Michael Raju,^{1,2,*} Baptiste Jayet,¹ and Stefan Andersson-Engels^{1,2}

¹*Tyndall National Institute, Lee Maltings Complex, Dyke Parade, Cork, Ireland, T12 R5CP*

²*School of Physics, University College Cork, College Road, Cork, Ireland, T12 K8AF*

We developed an open-source scalar wave transport model to estimate the generalized scattering matrix (S matrix) of a disordered medium in the diffusion regime. Here, the term generalization refers to the incorporation of evanescent wave field modes in addition to propagating modes while estimating the S matrix. For that we used the scalar Kirchhoff–Helmholtz boundary integral formulation together with the Green’s function perturbation method to generalize the conventional Fisher-Lee relations to include evanescent modes as well. The estimated S matrix, which satisfies generalized unitarity and reciprocity conditions, is modeled for a $2D$ disordered waveguide. The generalized transmission matrix contained in the S matrix is used to estimate the optimal phase-conjugate wavefront for focusing onto an evanescent mode. The phenomena of universal transmission value of $2/3$ for such an optimal phase conjugate wavefront is also shown in the context of evanescent wave mode focusing through a diffusive disorder. The presented code framework may be of interest to wavefront shaping researchers for visualizing and estimating wave transport properties in general.

I. INTRODUCTION

Coherent control[1] of waves in disordered media through wavefront shaping has been an actively researched topic in various domains of physics such as electromagnetics and acoustics. Experimental coherent control for focusing light outside a disordered medium[2], for enhancing total light transmission through a disorder[3, 4] and inside a region enclosed by disorder[5] have been reported. Preferential deposition[6–8] of energy inside a disorder has also been a potential application within the scope of the coherent control of light. Access to wave shaping devices such as spatial light modulators have helped to accelerate the research on coherent control experiments using light, especially using optical[9] or acousto-optical[5] transmission matrices. For the comprehensive study of the transport aspects of these wavefront shaping applications, modeling of the scattering matrix (S matrix) is particularly useful.

To estimate the regular S matrix containing only the propagating wave modes for wavefront shaping applications, the Green’s function perturbation method together with the conventional Fisher-Lee relations[1, 10], is used. Such a method is usually adopted to validate wavefront shaping experiments[3, 4, 11, 12] involving only propagating wave modes. A waveguide like geometry, usually associated with the Landauer formalism for electronic conduction[13], is typically adopted for the validation of the wavefront shaping experiments. On the other hand, accounting evanescent wave modes are also experimentally important in the context of wavefront shaping for achieving sub-wavelength resolution while focusing[14, 15]. These experiments involving the focusing on evanescent wave modes is backed and motivated by the first proposal of the generalized S matrix

by Carminati et al.[16] and the associated description of its unitarity and reciprocity properties. Here, the term generalization refers to the inclusion of evanescent modes in addition to the conventional propagating modes while estimating the S matrix. The overarching goals of this paper is 1) to describe the method used for numerically estimating the previously proposed generalized S matrix by Carminati et al.[16] for a disordered medium in the Landauer-waveguide geometry and 2) to combine the statistical analysis of scattered propagating and evanescent modes under the generalized modeling framework particularly targeting wavefront shaping applications. In addition to that, the classical wave scattering methods presented in the paper is coded in MATLAB[®] and it is available to the readers as an open source package along with its user manual. Hence, the interested readers can use the code not only for the numerical estimation of the generalized S matrix, but also for the general visualization of wave transport inside the medium especially involving propagating eigenchannels.

The paper is organized as the following. First, Sec. II reviews the definitions of the propagating and evanescent eigenmodes, the unperturbed and the disorder-perturbed Green’s functions based on which the S matrix is defined. For the disorder-perturbation of the Green’s function, spatially correlated disorders are utilized whose correlation length could be used to tailor the transport properties. Once the perturbed Green’s function is obtained, the Kirchhoff–Helmholtz boundary integral formulation of the wave scattering problem is discussed. Such a boundary integral formulation is used to estimate the generalized S matrix from the perturbed Green’s function. The boundary integral equation also helps to visualize the total field for a given incident wave from the left or the right side of the disorder and to validate the numerical correctness of the estimated generalized S matrix. Next, Sec. III presents the direct estimation of the generalized S matrix components from the perturbed Green’s function yielding the generalization of the conventional

* michaelraju@umail.ucc.ie

Fisher-Lee relations. To ensure the numerical correctness of the code implementation, the estimated S matrix is shown to satisfy the generalized unitary and reciprocity relations in the Sec. IV. These relations are also crucial for discussing the properties of focusing onto an evanescent mode, by the phase conjugation of the transmitted propagating wave. Towards the last portion of the paper (Sec. V), the scenario of wavefront shaping involving the focusing onto an evanescent mode in transmission and its associated properties, particularly the universal background transmission, are studied. Formation of a non-zero background intensity while focusing is well-studied[17] in the case involving propagating modes.

To maintain the conciseness of the paper, a supplementary material[18] is provided which contains derivations of some of the results presented in the paper. In addition to that, a user manual is also provided which summarizes various aspects of the code packages used to generate the results.

II. DEFINITIONS AND NOTATIONS USED FOR THE BOUNDARY INTEGRAL FORMULATION

The paper deals with the 2D scalar Helmholtz wave equation without loss or gain given as

$$[\nabla^2 + k_0^2 \mu_r \tilde{\epsilon}_r(r)] \tilde{E}(r) = 0, \quad (1)$$

where $\tilde{E}(r)$ denotes the complex valued 2D scalar wave field as a function of the position $r = (z, y)$, $k_0 = 2\pi/\lambda_0$ is the free-space wave vector magnitude, λ_0 the free-space wavelength, $\tilde{\epsilon}_r(r)$ the relative dielectric permittivity constant (as a function of the position) forming the scattering strength of the random media and μ_r (taken as unity) the relative permeability constant. The time harmonic dependence of $\tilde{E}(r)$ is implicitly taken as $e^{-i\omega_0 t}$ where i is the imaginary number and ω_0 the angular temporal frequency. The disorder dielectric constant $\tilde{\epsilon}_r(r)$ is defined as a spatially dependent perturbation $\delta\tilde{\epsilon}_r(r)$ against a uniform reference (background) dielectric constant value of $\tilde{\epsilon}_r^{ref}$ as $\tilde{\epsilon}_r(r) = \tilde{\epsilon}_r^{ref} + \delta\tilde{\epsilon}_r(r)$. In this paper, the $\delta\tilde{\epsilon}_r(r)$ taken is spatially correlated and one may refer to the Appendix Sec. A and the Supplementary Sec. I for the description regarding the generation of a spatially correlated disorder used for the modeling. Although the uncorrelated disorders with very small correlation length l_c (approaching zero) are analytically and computationally easier to implement, random media such as biological tissue samples involve a non-zero spatial correlation length[19]. If $\delta\tilde{\epsilon}_r(r) = 0$, then the wave equation for the disorder-less region takes the form $[\nabla^2 + k_{ref}^2] \tilde{E}(r) = 0$, where $k_{ref}^2 = k_0^2 \tilde{\epsilon}_r^{ref}$ such that $k_{ref} = k_0 \eta_{ref}$. Here, k_{ref} is the magnitude of the wave vector in a spatially uniform reference dielectric medium and $\eta_{ref} = \sqrt{\tilde{\epsilon}_r^{ref}}$, the refractive index of the reference medium.

Completely reflecting (mirror) boundary conditions at the transverse boundaries (at $y = 0$ and $y = W$ in

FIG. 1(a)) was implemented for the easy accounting of the flux conservation just at the left and the right longitudinal boundaries (at $z = z_L$ and $z = z_R$). The subscripts L and R on the boundary Γ denote the left and the right boundaries respectively as shown in the FIG. 1(a). With respect to the geometry shown in FIG. 1(a), without any disorder, one could define both propagating (shown in FIG. 1(b)) and evanescent (shown in FIG. 1(c) and FIG. (d)) wave states referred to as eigenmodes. These eigenmodes are the orthonormal basis wave states forming the modal basis with which any arbitrary wave existing in the computational domain can be expressed as a basis expansion. The S matrix is defined with respect to these eigenmode basis wave states where these wave field modes can be propagating (pr) or evanescent (ev) in general. Conventionally, the right travelling (along $+z$ direction) or the left travelling (along $-z$ direction) propagating eigenmodes are combinedly defined as

$$\psi_{m,pr}^\pm(z, y) = \Phi_{m,pr}^\pm(z) \chi_m(y), \quad (2)$$

where $\Phi_{m,pr}^\pm(z) = \frac{1}{\sqrt{k_z^{(m)}}} e^{\pm i k_z^{(m)} z}$ and $\chi_m(y) = \sqrt{\frac{2}{W}} \sin(k_y^{(m)} y)$ such that $k_y^{(m)} = m\pi/W$ is the transverse wave vector component of the m^{th} eigenmode along the y direction and $k_z^{(m)}$ is the real longitudinal wave vector component of the m^{th} eigenmode along the z direction. The “+” symbol on the superscript of $\Phi_{m,pr}^\pm(z, y)$ and $\psi_{m,pr}^\pm(z, y)$ denotes the wave propagation along $+z$ direction (from the left to the right of the computational domain) and the “-” symbol denotes the propagation along $-z$ direction (from the right to the left). Here, the function $\chi_m(y)$ is the transverse component of the eigenmode satisfying the mirror(reflection) boundary conditions (at $y = 0$ and $y = W$), with W being the transverse size of the computational region as shown in the FIG. 1(a). The index (m) as the superscript of $k_y^{(m)}$ denotes the positive integer index number for the m^{th} wave vector. (m) is a positive integer due to the discrete nature of the $k_y^{(m)}$ value occurring because of the transverse reflecting boundary condition. An example for the propagating eigenmode is plotted in FIG. 1(b) where $m = 3$ and the wave propagates rightwards. $\chi_m(y)$ obeys the orthogonality relationship $\langle \chi_m(y) | \chi_n(y) \rangle = \delta_{kron}(m, n)$, where δ_{kron} is the Kronecker delta function. There are approximately $2\eta_{ref}W/\lambda_0$ propagating eigenmodes. The wave vector components $k_y^{(m)}$ and $k_z^{(m)}$ obey the dispersion relation $(k_y^{(m)})^2 + (k_z^{(m)})^2 = k_{ref}^2$ where $k_{ref} = 2\pi\eta_{ref}/\lambda_0 = \omega_0\eta_{ref}/c$.

For the evanescent modes, $k_z^{(m)} = \sqrt{k_{ref}^2 - (k_y^{(m)})^2} = ik_{z,ev}^{(m)}$ are purely imaginary, where the term $k_{z,ev}^{(m)} = \sqrt{(k_y^{(m)})^2 - k_{ref}^2}$ is a real number. The left and right going evanescent eigenmodes, are defined to be originating out with respect to the two boundaries Γ_L and Γ_R

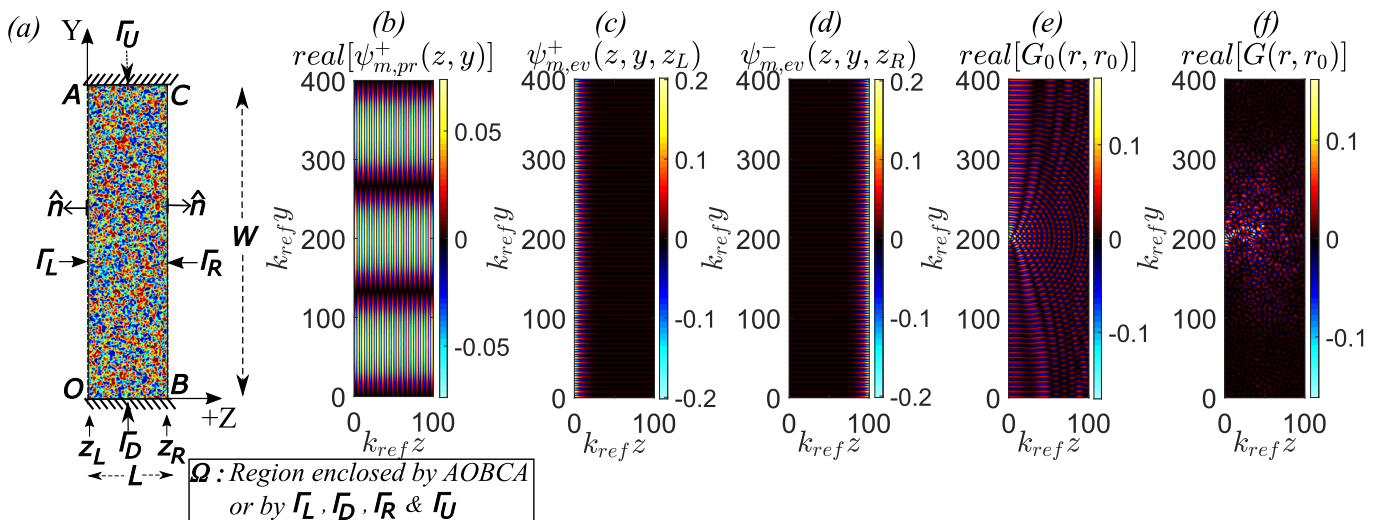


FIG. 1. **The waveguide-like geometry of the computational domain and the plots of the real parts of eigenmodes, unperturbed and perturbed Green's functions.** (a) Geometry of the computational domain. For the properties of the given spatially correlated diffusive disorder represented by the dielectric constant perturbation $\delta\epsilon_r(z, y)$, refer Appendix Sec. A. Boundary around the diffusive disorder (AOBCA) is denoted by Γ which is the union of four boundary segments Γ_L , Γ_D , Γ_R and Γ_U where L stands for left, R stands for right, U stands for up and D for down sides of the disorder. The 2D region enclosed by Γ is referred to as Ω . Transverse boundaries Γ_U and Γ_D have reflection (mirror) boundary conditions. The transverse size of the slab is W and the longitudinal thickness is L . (b) Real part of m^{th} eigenmode which is a propagating (pr) eigenmode. In this example, $m = 3$, out of the $M_{pr} = 130$ propagating modes possible for the given $k_{ref}W$. The $+$ symbol in the superscript denotes that the wave is propagating rightwards along $+z$ direction. The discrete form of the analytical equation given in Eq. 2 is used for plotting. (c) An evanescent eigenmode, plotted using Eq. 3a for $m = 132$, being the second evanescent mode out of the $M_{ev} = 30$ evanescent modes taken. Here, the evanescent mode is incident rightwards (with a superscript $+$) originating from the boundary Γ_L at z_L . Similarly, the left going scattered evanescent eigenmode exist at Γ_L in presence of disorder, although not plotted here. (d) An evanescent eigenmode (plotted using Eq. 3b for $m = 132$) incident leftwards (with a superscript $-$) originating from Γ_R at z_R . Similarly, the right going scattered evanescent mode exist at Γ_R in presence of disorder, although not plotted here. (e) Real part of the disorder-less Green's function $G_0(z, y, z_0, y_0)$ for $(k_{ref}z_0, k_{ref}y_0)$ at $(0, 201.46)$. Discrete form of Eq. 5 is used for plotting where 30 evanescent modes are used in addition to all the 130 propagating modes. (f) Similarly, plotting the perturbed Green's function $G(r, r_0)$ (corresponding to the disorder given in FIG. 5) estimated by solving the Dyson's equation (Eq. 6) as given in Supplementary Sec. II.

(boundaries shown in the FIG. 1(a) at z_L and z_R), held close to the disorder. These evanescent modes attenuate along the direction of incidence onto the disorder from the left side or the right side of the disorder and also attenuate while being scattered away. These evanescent modes are defined as the following with dependence on z_L or z_R ,

$$\psi_{m,ev}^{\pm}(z, y, z_L) = \Phi_{m,ev}^{\pm}(z, z_L)\chi_m(y), \quad (3a)$$

$$\psi_{m,ev}^{\pm}(z, y, z_R) = \Phi_{m,ev}^{\pm}(z, z_R)\chi_m(y), \quad (3b)$$

where

$$\Phi_{m,ev}^{\pm}(z, z_L) = \frac{1}{\sqrt{k_{z,ev}^{(m)}}} e^{-k_{z,ev}^{(m)}|z-z_L|} \quad (4a)$$

$$\text{and } \Phi_{m,ev}^{\pm}(z, z_R) = \frac{1}{\sqrt{k_{z,ev}^{(m)}}} e^{-k_{z,ev}^{(m)}|z-z_R|} \quad (4b)$$

The symbol “ \pm ” on the L.H.S of Eq. 4 indicates the directions of incidence/scattering of the evanescent mode originating relative to z_L or z_R , (with “ $+$ ” for rightward and “ $-$ ” for leftward emergence). Note that “ \pm ”

doesn't appear on R.H.S of Eq. 4 as both the leftward and rightward emerging modes are attenuating away from z_L or z_R along z . Two examples of the incident evanescent modes are given in FIG. 1(c) and FIG. 1(d), consisting of a right going evanescent eigenmode at Γ_L and a left going evanescent eigenmode at Γ_R , respectively. Although not plotted, similarly there exist scattered evanescent modes from the disorder which are left going at Γ_L and a right going at Γ_R .

The eigenmodes referred to as ψ_m in general, include a normalization factor $1/\sqrt{|k_z^{(m)}|}$. For the propagating modes, the normalization factor $1/\sqrt{k_z^{(m)}}$ ensures that the flux (current) component flowing normal to a given boundary region Γ_L or Γ_R , is unity. The flux density of the m^{th} eigenmode is defined as $\vec{J}^{(m)}(z, y) = J_z^{(m)}(r)\hat{e}_z + J_y^{(m)}(r)\hat{e}_y = \text{Im}\{\psi_m^* \nabla \psi_m\}$ where \hat{e}_z and \hat{e}_y are unit vectors along Z and Y respectively, and Im refers to the imaginary part. As there is no flux crossing along the transverse boundaries Γ_U and Γ_D , $J_y^{(m)}(r)$ is zero along the boundary-normal. For the evanescent modes, as

there is no flux crossing the boundaries, physically there is no need for defining a normalization factor. Nevertheless, a normalization factor $1/\sqrt{|k_z^{(m)}|} = 1/\sqrt{k_{z,ev}^{(m)}}$ is included in the definition for the evanescent eigenmodes. This is mainly for the convenience of modeling the propagating modes and the evanescent modes, to be of the same numerical order of magnitude to avoid precision errors while estimating the S matrix.

Next, using the propagating and evanescent eigenmodes, the analytical expression [20] for the 2D Green's function $G_0(r, r_0)$ (plotted in FIG. 1(e)) without any disorder perturbation is given as

$$G_0(z, y, z_0, y_0) = \sum_{m=1}^{\infty} \frac{1}{2ik_z^{(m)}} e^{ik_z^{(m)}|z-z_0|} \sqrt{\frac{2}{W}} \sin(k_y^{(m)}y) \sqrt{\frac{2}{W}} \sin(k_y^{(m)}y_0), \quad (5)$$

where $r_0 = (z_0, y_0)$ is the source location, $k_z^{(m)}$ is real for the propagating summation terms and $k_z^{(m)} = ik_{z,ev}^{(m)}$ is imaginary for the evanescent components. Although the summation in Eq. 5 runs from $m = 1$ to a large number, the summation is truncated such that it includes all the M_{pr} propagating modes where $M_{pr} \approx 2\eta_{ref}W/\lambda_0$ and a certain truncation number of evanescent modes, M_{ev} . As an example, in this paper, M_{ev} is set as 30, $M_{pr} = 130$ and $M_{total} = M_{pr} + M_{ev}$. Hence, numerically, the summation in Eq. 5 runs from $m = 1$ to $m = M_{total}$ while implementing $G_0(r, r_0)$ in the code. Using $G_0(r, r_0)$ and the dielectric disorder perturbation $\delta\tilde{\epsilon}_r(r)$ (shown in FIG. 5(a)), the perturbed Green's function $G(r, r_0)$ (plotted in FIG. 1(f)) is estimated using the Dyson's equation[13, 21] as given below.

$$G(r, r_0) = G_0(r, r_0) + \int_{r_1} G_0(r, r_1)V(r_1)G(r_1, r_0)dr_1, \quad (6)$$

where $V(r) = -k_0^2\delta\tilde{\epsilon}_r(r)$ is the scattering potential at the position r . The Dyson's integral equation is solved in this paper by generalizing the method given in [22, 23], by solving for a block of scattering particles taken at once and iteratively updating the Green's function. For details on the method used to obtain $G(r, r_0)$, refer Supplementary Sec. II.

As the propagating and the evanescent eigenmodes $\psi_m^{\pm}(r)$ form a complete basis set, the perturbed Green's function $G(r, r_0)$ can also be expanded in terms of these eigenmodes. On the left boundary, $G(r, r_0)$ can be expanded in terms of left going eigenmodes and on the right boundary, $G(r, r_0)$ can be expanded in terms of right going eigenmodes. Hence, $G(r, r_0)$ satisfies the homogeneous boundary conditions given in the Supplementary Sec. III, which is also satisfied by the eigenmodes. These boundary conditions are useful for simplifying the analysis to be presented in the following section. Next section deals with the Kirchhoff-Helmholtz boundary integral formulation of the scattering problem, incorporating $G(r, r_0)$ and the total field around the boundary Γ .

This is followed by the direct numerical estimation of the generalized S matrix from $G(r, r_0)$.

The goal in this section would be to establish the relationship between the perturbed Green's function $G(z, y, z_0, y_0)$ and the total wave field $\tilde{E}(z, y)$ existing inside and around a medium due to an arbitrary wave getting incident on the disorder. This helps to estimate the response of a random medium excited using an arbitrary incident wave. First, let the case of the wave incidence on the sample only from the left side be considered where $E^{inc}(z, y)$ (travelling from the left to right) is the incident wave. On the left boundary Γ_L , the total wave field due to wave incidence only on the left side is given as

$$\tilde{E}(z, y)|_{(z,y)\in\Gamma_L} = \tilde{E}^{inc}(z, y)|_{(z,y)\in\Gamma_L} + \tilde{E}^{refl}(z, y)|_{(z,y)\in\Gamma_L} \quad (7)$$

such that $\tilde{E}^{refl}(z, y)|_{(z,y)\in\Gamma_L}$ is the reflected wave on Γ_L . $\tilde{E}^{inc}(z, y)$ and $\tilde{E}^{refl}(z, y)$ can be expanded in terms of eigenmodes and their associated complex coefficients on Γ_L as the following.

$$\begin{aligned} \tilde{E}^{inc}(z, y)|_{(z,y)\in\Gamma_L} &= \sum_{m=1}^{M_{total}} c_m^+ \psi_m^+(z, y)|_{(z,y)\in\Gamma_L} \quad (8) \\ &= \sum_{m=1}^{M_{total}} c_m^+ \chi_m(y) \phi_m^+(z)|_{(z,y)\in\Gamma_L} \\ \text{such that } \phi_m^+(z) &= \begin{cases} \phi_{m,pr}^+(z) & \text{when } m \leq M_{pr} \\ \phi_{m,ev}^+(z, z_L) & \text{when } m > M_{pr} \end{cases} \end{aligned}$$

where $M_{total} = M_{pr} + M_{ev}$ is the total number of eigenmodes considered and particularly $k_z^{(m)} = ik_{z,ev}^{(m)}$ when $m > M_{pr}$. Here, c_m^+ is the m^{th} complex coefficient used to synthesize the incident wave in terms of eigenmodes propagating along the $+z$ direction. Similarly,

$$\begin{aligned} \tilde{E}^{refl}(z, y)|_{(z,y)\in\Gamma_L} &= \sum_{n=1}^{N_{total}} r_n^- \psi_n^-(z, y)|_{(z,y)\in\Gamma_L} \quad (9) \\ &= \sum_{n=1}^{N_{total}} r_n^- \chi_n(y) \phi_n^-(z)|_{(z,y)\in\Gamma_L} \\ \text{such that } \phi_n^-(z) &= \begin{cases} \phi_{n,pr}^-(z) & \text{when } n \leq N_{pr} \\ \phi_{n,ev}^-(z, z_L) & \text{when } n > N_{pr} \end{cases} \\ \text{and } r_n^- &= \sum_{m=1}^{M_{total}} S_{11}^{nm} c_m^+ \end{aligned}$$

where S_{11}^{nm} are the elements of the generalized reflection matrix S_{11} for the wave incidence only from the left side of the disorder. m as the index denotes the incident eigenmode number and n denotes the scattered eigenmode number.

On the right boundary Γ_R , only the transmitted wave $\tilde{E}^{trans}(z, y)|_{(z,y)\in\Gamma_R}$ exists, for the scenario of wave incidence only on the left side of the disorder. Therefore, the

total field on Γ_R is given as

$$\begin{aligned} \tilde{E}(z, y)|_{(z, y) \in \Gamma_R} &= \tilde{E}^{trans}(z, y)|_{(z, y) \in \Gamma_R} \\ &= \sum_{n=1}^{N_{total}} t_n^+ \phi_n^+(z) \chi_n(y)|_{(z, y) \in \Gamma_R} \end{aligned} \quad (10)$$

$$\text{such that } \phi_n^+(z) = \begin{cases} \phi_{n,pr}^+(z) & \text{when } n \leq N_{pr} \\ \phi_{n,ev}^+(z, z_R) & \text{when } n > N_{pr} \end{cases}$$

$$\text{and } t_n^+ = \sum_{m=1}^{M_{total}} S_{21}^{nm} c_m^+,$$

where S_{21}^{nm} are the elements of the generalized transmission matrix S_{21} for the wave incidence only from the left side of the disorder.

Inside the medium, the total field of the wave is denoted as $\tilde{E}(z, y)$ itself. Consider the Helmholtz equation for the Green's function and also for the total field as the following,

$$[\nabla^2 + k_0^2 \tilde{\epsilon}_r(z, y)]G(z, y, z_0, y_0) = \delta(z, z_0)\delta(y, y_0), \quad (11)$$

$$[\nabla^2 + k_0^2 \tilde{\epsilon}_r(z, y)]\tilde{E}(z, y) = 0, \quad (12)$$

where ∇^2 is the Laplacian operator with respect to the field position (z, y) . In Eq. 11, (z_0, y_0) is the Dirac-delta source location. Multiplying Eq. 11 using $\tilde{E}(z, y)$ and Eq. 12 using $G(z, y, z_0, y_0)$, followed by subtraction and the use of divergence theorem, the following Kirchhoff-Helmholtz boundary integral equation is obtained as given in the appendix Sec. A of [24],

$$\begin{aligned} \tilde{E}(z_0, y_0)|_{(z_0, y_0) \in \Omega} &= \\ &= \iint_{\Gamma} \nabla \cdot \left\{ \tilde{E}(r) \nabla G(r, r_0) - G(r, r_0) \nabla \tilde{E}(r) \right\} dz dy \\ &= \int_{\Gamma} \left\{ \tilde{E}(r) \nabla G(r, r_0) - G(r, r_0) \nabla \tilde{E}(r) \right\} \cdot \hat{n} d\Gamma, \end{aligned} \quad (13)$$

where r denotes (z, y) and r_0 denotes (z_0, y_0) . Also, note that now (z_0, y_0) is the location in which the field is visualized and it is not the source location any more. This is consistent with the fact that Green's function has the reciprocity property of $G(r, r_0) = G(r_0, r)$. As there is no flux crossing Γ_U and Γ_D , the above given boundary integral involves only the terms associated with Γ_L and Γ_R . The Kirchhoff-Helmholtz boundary integral equation implies that the total field $\tilde{E}(z_0, y_0)$ at a point (z_0, y_0) inside the closed region Ω bounded by Γ can be estimated, if the value of $\tilde{E}(z, y)$ and the Green's function $G(z, y, z_0, y_0)$, together with its spatial derivatives, are known at the boundaries Γ_L and Γ_R . The boundary integral can be simplified (derivation of which is given in the Supplementary Sec. IV) as the following. For the wave incidence only from the left to right of the disorder (incidence onto Γ_L),

$$\begin{aligned} \tilde{E}(z_0, y_0)|_{(z_0, y_0) \in \Omega} &= \\ &= \sum_{m=1}^{M_{total}} 2ik_z^{(m)} \int \tilde{E}_m^{inc}(z, y) G(z, y, z_0, y_0)|_{(z, y) \in \Gamma_L} dy \end{aligned} \quad (14)$$

where $\tilde{E}_m^{inc}(z, y)|_{(z, y) \in \Gamma_L} = c_m^+ \psi_m^+(z, y)|_{(z, y) \in \Gamma_L}$, M_{total} , the total number of eigenmodes considered and particularly $k_z^{(m)} = ik_{z,ev}^{(m)}$ when $m > M_{pr}$. Here, c_m^+ is the m^{th} complex coefficient used to synthesize the incident wave in terms of eigenmodes propagating along the $+z$ direction.

Similarly, for wave incidence only from the right side of the disorder (incidence onto Γ_R), the equation is similar to that of Eq. 14, except that now $(z, y) \in \Gamma_R$.

$$\begin{aligned} \tilde{E}(z_0, y_0)|_{(z_0, y_0) \in \Omega} &= \\ &= \sum_{m=1}^{M_{total}} 2ik_z^{(m)} \int \tilde{E}_m^{inc}(z, y) G(z, y, z_0, y_0)|_{(z, y) \in \Gamma_R} dy \end{aligned} \quad (15)$$

where $\tilde{E}_m^{inc}(z, y)|_{(z, y) \in \Gamma_R} = c_m^- \psi_m^-(z, y)|_{(z, y) \in \Gamma_R}$ and particularly $k_z^{(m)} = ik_{z,ev}^{(m)}$ when $m > M_{pr}$. Here, similar to that of Eq. 8,

$$\tilde{E}^{inc}(z, y)|_{(z, y) \in \Gamma_R} = \sum_{m=1}^{M_{total}} c_m^- \psi_m^-(z, y)|_{(z, y) \in \Gamma_R}. \quad (16)$$

The simplified boundary integral equations Eq. 14 or Eq. 15 can be used for two purposes. 1) The generalized reflection (S_{11} and S_{22}) and transmission (S_{21} and S_{12}) matrices can be estimated. 2) The boundary integral equations can be used for visualizing the total field $\tilde{E}(z_0, y_0)|_{(z_0, y_0) \in \Omega}$, for a given incident wave from the left side or the right side of the disorder. As an example, in Supplementary Sec. VI, the transmission eigenchannels associated with $S_{21}^{pr,pr}$ and $S_{12}^{pr,pr}$ are plotted using the boundary integral equations.

Next section explains how the boundary integral equations are used to estimate the generalized S matrix where the traditional Fisher-Lee method[1, 10, 24, 25] is generalized to include the evanescent wave modes as well. The definition of S matrix (an estimated example is shown in FIG. 2(a)) is given as

$$S = \begin{bmatrix} S_{11} & S_{12} \\ S_{21} & S_{22} \end{bmatrix}, \quad (17)$$

where S_{21} and S_{12} are generalized transmission matrices for wave incidence from the left and right, respectively. Similarly, S_{11} and S_{22} are the generalized reflection matrices for wave incidence from the left and right, respectively. The size of the transmission matrix S_{21} is generally given as $[N_{total} \times M_{total}]$ where $M_{total} = M_{pr} + M_{ev}$ is the number of incident eigenmodes and $N_{total} = N_{pr} + N_{ev}$ the number of transmitted eigenmodes. For the quasi-1D geometry shown in FIG. 1(a), $M_{pr} = N_{pr}$ and $M_{ev} = N_{ev}$.

III. EXTENDED FISHER-LEE RELATIONS FOR ESTIMATING THE GENERALIZED S MATRIX

Due to the wave incidence from the left side of the disorder onto the boundary Γ_L , there exist the total field

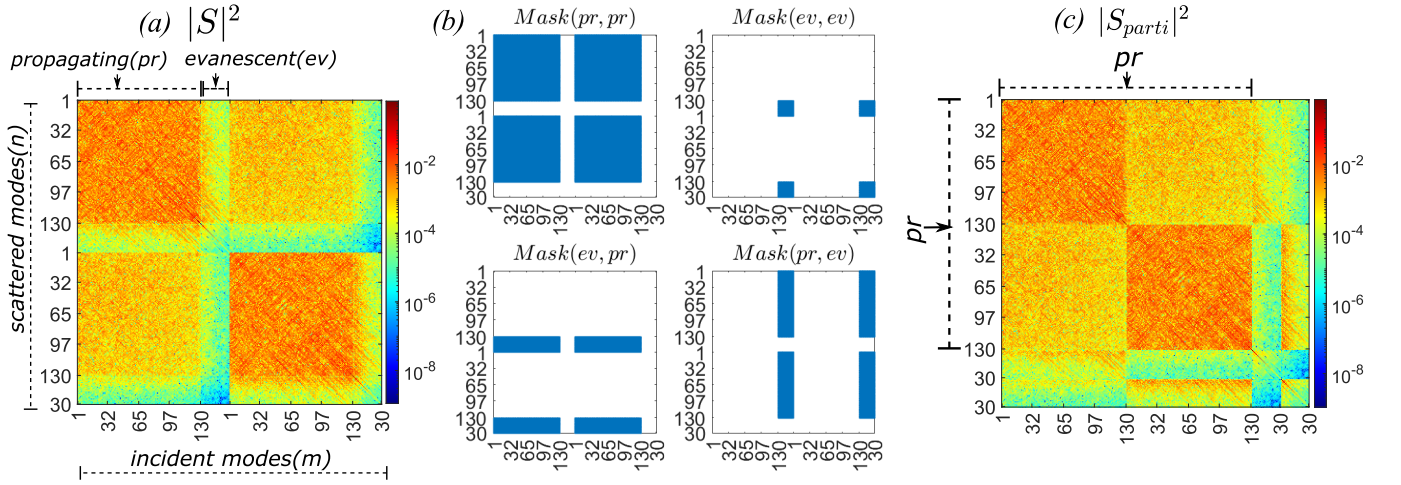


FIG. 2. **Plotting the S matrix of a diffusive disorder with average transmission $\langle \tau_{21}^{pr,pr} \rangle = 0.198$.** (a) Squared magnitude of the S matrix given in Eq. 17 (plotted in \log scale) estimated using the generalized Fisher-Lee relations given in Tables I, II, III, and IV. Spatially correlated disorder shown in FIG. 5 is used. The number of propagating modes (M_{pr}) involved for wave incidence and scattering is 130 and the number of evanescent modes (M_{ev}) is 30 for the quasi-1D geometry. As an example, the S_{11} portion of the S matrix, contains both propagating and evanescent wave modes where the propagating modes appear first in the matrix (with respect to row and column indices) followed by the evanescent modes. (b) Plotting the sparsity of the selection mask matrix (blue colour stands for unity and white for zeros) used to re-arrange the S matrix given in (a) to form the partitioned S matrix (S_{parti}) based on [26]. As an example, $mask(ev, pr)$ selects that part of the S matrix which contains only modes such that the incident modes are propagating and the scattered being evanescent. (c) Squared magnitude of the partitioned S matrix [26] (in \log scale) is shown where the matrix elements of the S matrix given in (a) are rearranged using the selection mask given in (b) to obtain the form given in Eq. 22. S_{parti} will be used later (as shown in the FIG. 3) to numerically validate the generalized unitarity and reciprocity relations.

due to the incident wave and the reflected wave on Γ_L . On the transmitted side, there exist the transmitted wave field which is the total wave. One could match the total field with respect to the boundary integral equation and solve for S_{11} and S_{21} , to obtain the generalized Fisher-Lee relations. Similarly, the estimation of S_{22} and S_{12} follow the same logic where the wave incidence is from the right side of the disorder. The derivations for the generalized S_{11} , S_{21} , S_{22} and S_{12} , given by the generalized Fisher-Lee relations are provided in Supplementary Sec. V. Those relations are summarized as the following.

For the estimation of S_{11} , $(z = 0, y) \in \Gamma_L$ & $(z_0 = 0, y_0) \in \Gamma_L$. Let there be an integral defined as the following,

$$G_{nm}^{S_{11}} = \int \int \chi_m(y) G(z, y, z_0, y_0) \chi_n(y_0) dy dy_0 |_{(z,y) \in \Gamma_L \& (z_0,y_0) \in \Gamma_L} \quad (18)$$

which can be interpreted as a Fourier-like decomposition in the eigenspace, of the Green's function component used for estimating S_{11} . Then, S_{11} in terms of $G_{nm}^{S_{11}}$, is given in the Table I. The terms under $Inc(m)$ denotes the nature of the m^{th} incident wave mode and $Refl(n)$ the nature of the n^{th} reflected wave mode, being propagating (pr) or evanescent (ev). For the estimation of S_{21} , $(z = 0, y) \in \Gamma_L$ & $(z_0 = z_R, y_0) \in \Gamma_R$. Let there be

TABLE I. Elements of S_{11}

$Inc(m)$	$Refl(n)$	S_{11}^{nm}
pr	pr	$-\delta_{k_{ron}}(n, m) + 2i\sqrt{k_z^{(m)}}\sqrt{k_z^{(n)}}G_{nm}^{S_{11}}$
ev	ev	$-\delta_{k_{ron}}(n, m) - 2\sqrt{ k_z^{(m)}}\sqrt{ k_z^{(n)}}G_{nm}^{S_{11}}$
pr	ev	$2i\sqrt{k_z^{(m)}}\sqrt{ k_z^{(n)}}G_{nm}^{S_{11}}$
ev	pr	$-2\sqrt{ k_z^{(m)}}\sqrt{k_z^{(n)}}G_{nm}^{S_{11}}$

an integral defined as

$$G_{nm}^{S_{21}} = \int \int \chi_m(y) G(z, y, z_0, y_0) \chi_n(y_0) dy dy_0 |_{(z,y) \in \Gamma_L \& (z_0,y_0) \in \Gamma_R} \quad (19)$$

Then, S_{21} in terms of $G_{nm}^{S_{21}}$ is given in the Table II.

For evaluating S_{22} and S_{12} , incident wave propagates from right side onto Γ_R . Hence, the total field on Γ_R consists of incident wave and the reflected wave. The total field on Γ_L is the transmitted wave propagating to the left side of the disorder. For the estimation of S_{22} , $(z = z_R, y) \in \Gamma_R$ and $(z_0 = z_R, y_0) \in \Gamma_R$. Let there be

TABLE II. Elements of S_{21}

$Inc(m)$	$Trans(n)$	S_{21}^{nm}
pr	pr	$2i\sqrt{k_z^{(m)}}\sqrt{k_z^{(n)}}e^{-iz_R k_z^{(n)}}G_{nm}^{S_{21}}$
ev	ev	$-2\sqrt{ k_z^{(m)} }\sqrt{ k_z^{(n)} }G_{nm}^{S_{21}}$
pr	ev	$2i\sqrt{k_z^{(m)}}\sqrt{ k_z^{(n)} }G_{nm}^{S_{21}}$
ev	pr	$-2\sqrt{ k_z^{(m)} }\sqrt{k_z^{(n)}}e^{-iz_R k_z^{(n)}}G_{nm}^{S_{21}}$

an integral defined

$$G_{nm}^{S_{22}} = \iint \chi_m(y)G(z, y, z_0, y_0)\chi_n(y_0)dydy_0|_{(z,y)\in\Gamma_R \& (z_0,y_0)\in\Gamma_L} \quad (20)$$

Then, S_{22} in terms of $G_{nm}^{S_{22}}$ is given in the Table III. For the evaluation of S_{12} , $(z, y) \in \Gamma_R$ & $(z_0, y_0) \in \Gamma_L$

TABLE III. Elements of S_{22}

$Inc(m)$	$Ref1(n)$	S_{22}^{nm}
pr	pr	$-\delta_{kron}(n, m)e^{-iz_R(k_z^{(m)}+k_z^{(n)})} + 2i\sqrt{k_z^{(n)}}\sqrt{k_z^{(m)}}e^{-iz_R(k_z^{(m)}+k_z^{(n)})}G_{nm}^{S_{22}}$
ev	ev	$-\delta_{kron}(n, m) - 2\sqrt{ k_z^{(m)} }\sqrt{ k_z^{(n)} }G_{nm}^{S_{22}}$
pr	ev	$+2i\sqrt{k_z^{(m)}}\sqrt{ k_z^{(n)} }e^{-iz_R k_z^{(m)}}G_{nm}^{S_{22}}$
ev	pr	$-2\sqrt{ k_z^{(m)} }\sqrt{k_z^{(n)}}e^{-iz_R k_z^{(n)}}G_{nm}^{S_{22}}$

and define the integral

$$G_{nm}^{S_{12}} = \iint \chi_m(y)G(z, y, z_0, y_0)\chi_n(y_0)dydy_0|_{(z,y)\in\Gamma_R \& (z_0,y_0)\in\Gamma_L} \quad (21)$$

Finally, S_{12} in terms of $G_{nm}^{S_{12}}$ is given in the Table IV. Tables I,II,III and IV are the main results of this section.

IV. VERIFICATION OF THE GENERALIZED UNITARITY AND RECIPROCITY PROPERTIES

In this section, the generalized reciprocity relations[16, 26] are summarized for the Landauer-waveguide geometry by comparing the expressions for $S_{11}, S_{21}, S_{22}, S_{12}$ between Tables I,II,III and IV, respectively. Comparing the expression given in the first two rows of all the tables where m and n are either both propagating or both

TABLE IV. Elements of S_{12}

$Inc(m)$	$Trans(n)$	S_{12}^{nm}
pr	pr	$2i\sqrt{k_z^{(m)}}\sqrt{k_z^{(n)}}e^{-iz_R k_z^{(m)}}G_{nm}^{S_{12}}$
ev	ev	$-2\sqrt{ k_z^{(m)} }\sqrt{ k_z^{(n)} }G_{nm}^{S_{12}}$
pr	ev	$2i\sqrt{k_z^{(m)}}\sqrt{ k_z^{(n)} }e^{-iz_R k_z^{(m)}}G_{nm}^{S_{12}}$
ev	pr	$-2\sqrt{ k_z^{(m)} }\sqrt{k_z^{(n)}}G_{nm}^{S_{12}}$

evanescent, we get $S_{11}^{nm} = S_{11}^{mn}$, $S_{22}^{nm} = S_{22}^{mn}$, and $S_{21}^{nm} = S_{12}^{mn}$. This is due to the perturbed Green's function reciprocity symmetry such that $G(r, r_0) = G(r_0, r)$ implying $G_{nm} = G_{mn}$. On the other hand, when $m \leq M_{pr}$ and $n > N_{pr}$, then $S_{11}^{mn} = iS_{11}^{nm}$, $S_{22}^{mn} = iS_{22}^{nm}$, $S_{12}^{mn} = iS_{21}^{nm}$ and $S_{21}^{mn} = iS_{12}^{nm}$ where the factor of i has to be incorporated. It also implies that, when $m > M_{pr}$ and $n \leq N_{pr}$, then $S_{11}^{mn} = -iS_{11}^{nm}$, $S_{22}^{mn} = -iS_{22}^{nm}$, $S_{12}^{mn} = -iS_{21}^{nm}$ and $S_{21}^{mn} = -iS_{12}^{nm}$, where the factor of $-i$ has to be incorporated. Hence, the generalized reciprocity relations are numerically validated in the matrix form as shown in FIG. 3(a). Among that the important reciprocity relations relevant to this paper are $S_{12}^{pr, ev} = i(S_{21}^{ev, pr})^T$ and $S_{12}^{pr, pr} = (S_{21}^{pr, pr})^T$.

Next is the verification of the unitarity property of the S matrix which implies flux conservation. For convenience of representation, the partitioned S matrix (S_{parti}) has been defined[26] to compactly evaluate the unitarity relationship. S_{parti} rearranges the S matrix defined in Eq. 17 to the following block-matrix form

$$\begin{pmatrix} c_{out}^{pr} \\ c_{out}^{ev} \end{pmatrix} = \underbrace{\begin{bmatrix} S_{parti}^{pr, pr} & S_{parti}^{pr, ev} \\ S_{parti}^{ev, pr} & S_{parti}^{ev, ev} \end{bmatrix}}_{S_{parti}} \begin{pmatrix} c_{inc}^{pr} \\ c_{inc}^{ev} \end{pmatrix} \quad (22)$$

where the terms (in the superscript of the submatrices) pr in the short-form stands for the propagating and ev stands for the evanescent modes. The first index in the superscript denotes the nature of the outgoing scattered modes and the second index denotes nature of the incident modes. Also, the coefficients associated with the incident(subscript inc) and outgoing(subscript out) scattered eigenmodes are separated into the propagating and the evanescent modes. As an example, $S_{parti}^{pr, ev}$ contains those elements of the S matrix, which have incident modes being evanescent and outgoing modes being propagating, grouped together as shown in FIG. 2(c). A selection mask used to crop the S matrix to yield the S_{parti} is given in FIG. 2(b). Then, the compact form[26, 27] of the generalized unitarity relation, $S_{parti}^\dagger I_{pr} S_{parti} = I_{pr} + i \{ S_{parti}^\dagger I_{ev} - I_{ev} S_{parti} \}$, is used for the numerical validation of the generalized unitarity in this paper, as shown in FIG. 3(b). Here I_{pr}

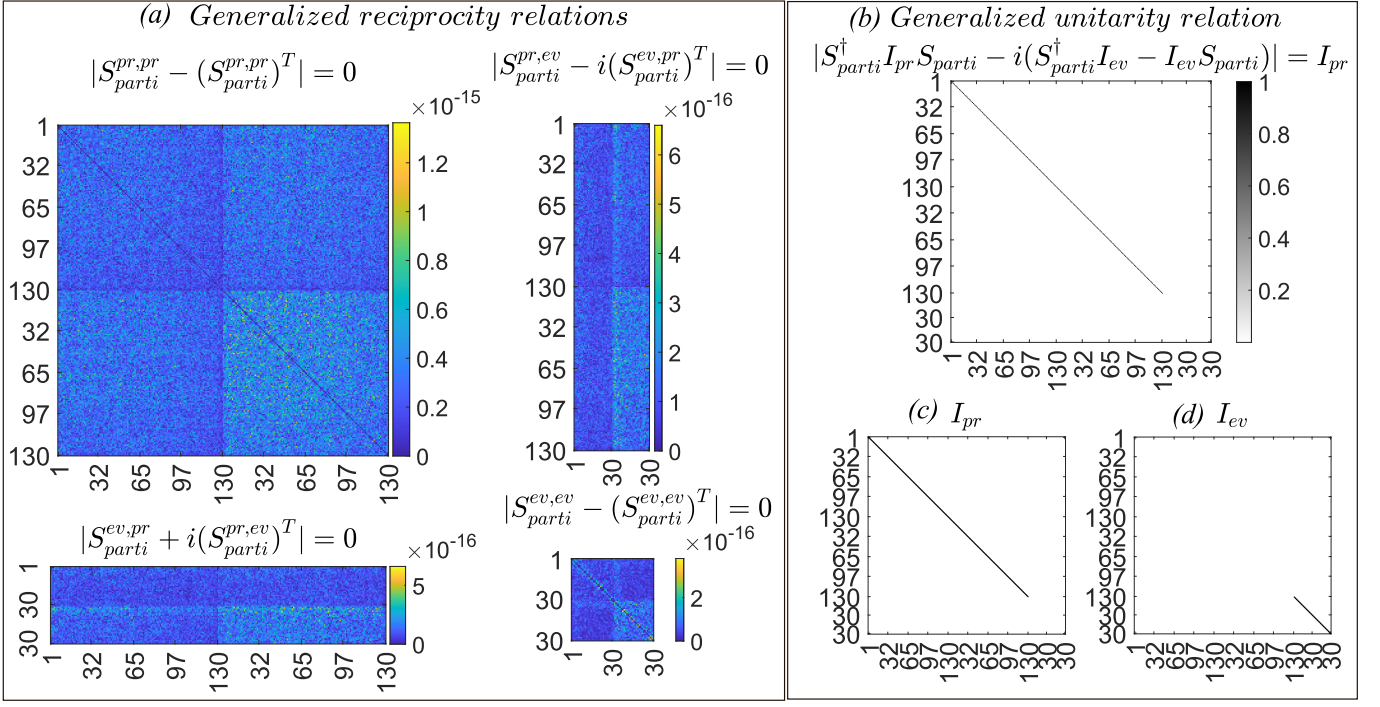


FIG. 3. **Numerical validation of the generalized unitarity and reciprocity relations.** (a) Plotting the magnitude of the numerically estimated generalized reciprocity relations in terms of S_{parti} . The modulus terms on the L.H.S of the reciprocity relations are plotted whose magnitudes are of the order of 10^{-15} , approximately equal to zero. T stands for matrix transpose. (b) Plotting the magnitude of the numerically estimated generalized unitarity relation based on the analytical result given in [26, 27]. The modulus term on the L.H.S of the unitarity relation is plotted. The non-zero diagonal elements inside the modulus term on the L.H.S (shown in black colour) are all unities and the magnitude of all the other elements are of the order of 10^{-13} , approximated to zero. \dagger stands for the conjugate transpose. For additional numerical verification involving the expanded forms of the compact unitarity relation, refer to supplementary FIG. 3. (c) Plotting the sparsity of the matrices I_{pr} and (d) I_{ev} defined in relation to the S_{parti} used in the unitarity relation (black colour stands for unity and white for zeros).

is a matrix with unity only on the diagonal corresponding to the purely-propagating portion of S_{parti} and zeros elsewhere, as shown in the FIG. 3(c). Similarly, I_{ev} contains unity elements only on the diagonal corresponding to the evanescent portion of S_{parti} , also shown in FIG. 3(d). The compact form[26, 27] of the generalized unitary relation is the combination of the following relations, $(S_{parti}^{pr,pr})^\dagger S_{parti}^{pr,pr} = I$, $(S_{parti}^{pr,pr})^\dagger S_{parti}^{pr,ev} = i(S_{parti}^{ev,pr})^\dagger$ and $(S_{parti}^{pr,ev})^\dagger S_{parti}^{pr,ev} = i \left\{ (S_{parti}^{ev,ev})^\dagger - S_{parti}^{ev,ev} \right\}$.

Flux conservation in terms of the modal coefficients given in Eq. 22, is explained next. The complex vector c_{inc} and c_{out} with its elements being the complex modal coefficients defined before

$$c_{inc} = \begin{pmatrix} c_{inc}^{+,L} \\ c_{inc}^{-,R} \\ c_{inc}^- \end{pmatrix} \text{ and } c_{out} = \begin{pmatrix} r_{out}^{-,L} \\ t_{out}^{+,R} \\ c_{out}^- \end{pmatrix} \quad (23)$$

where $c_{inc}^{+,L}$ is the column vector containing the modal coefficients of the right going (+) incident wave incident on Γ_L . Similarly, the column vector $c_{inc}^{-,R}$ contains the modal coefficients of the left going (-) incident wave incident on Γ_R . Also, $r_{out}^{-,L}$ is the column vector containing the modal coefficients of the outgoing wave emerging from Γ_L , due

to the wave incidence from both the left and the right side of the disorder. Likewise, $t_{out}^{+,R}$ is the column vector containing the modal coefficients of the outgoing wave emerging from Γ_R due to the wave incidence from both the left and the right side of the disorder. The propagating and the evanescent portion of c_{inc} can be separated out as c_{inc}^{pr} and c_{inc}^{ev} as the following, which are used in the Eq. 22.

$$c_{inc}^{pr} = \begin{pmatrix} c_{inc}^{+,L,pr} \\ c_{inc}^{-,R,pr} \\ c_{inc}^- \end{pmatrix} \text{ and } c_{inc}^{ev} = \begin{pmatrix} c_{inc}^{+,L,ev} \\ c_{inc}^{-,R,ev} \\ c_{inc}^- \end{pmatrix} \quad (24)$$

Similarly, the propagating and the evanescent portion of c_{out} can be separated out as c_{out}^{pr} and c_{out}^{ev} .

The flux conservation method given in [16, 26] can be applied onto the modal coefficients. It implies that the incident flux $F_{inc} = \int_0^W \text{Im} \left\{ \tilde{E}_{inc}^* \frac{\partial}{\partial z} \tilde{E}_{inc} \right\} dy$ should be equal to the outgoing flux $F_{out} = \int_0^W \text{Im} \left\{ \tilde{E}_{out}^* \frac{\partial}{\partial z} \tilde{E}_{out} \right\} dy$ such that $F_{inc} = F_{out}$. It results in the following generalized flux conservation relation for the Landauer-waveguide geometry, which is same in essence to that of [16, 26] defined for a different geom-

etry involving angular spectrum representation.

$$(c_{inc}^{pr})^\dagger c_{inc}^{pr} - (c_{out}^{pr})^\dagger c_{out}^{pr} = i \left\{ (c_{inc}^{ev})^\dagger c_{out}^{ev} - (c_{out}^{ev})^\dagger c_{inc}^{ev} \right\} \quad (25)$$

For the conventional scenario of purely-propagating incident and scattered modes, the R.H.S of the Eq. 25 is zero as $c_{inc}^{ev} = 0$ and $c_{out}^{ev} = 0$, implying the well-known propagating-flux conservation that $(c_{inc}^{pr})^\dagger c_{inc}^{pr} = (c_{out}^{pr})^\dagger c_{out}^{pr}$, meaning that the incident flux, $(c_{inc}^{pr})^\dagger c_{inc}^{pr}$ is the same as the outgoing scattered flux $(c_{out}^{pr})^\dagger c_{out}^{pr}$. For a purely evanescent incident wave, $c_{inc}^{pr} = 0$. Then, the Eq. 25 implies that, the outgoing propagating flux (on the *L.H.S*) occurs due to the counter-propagating interference of evanescent modes (on the *R.H.S*) proposed in[16] and discussed in [26, 28]. Here, the counter propagating interference is defined between incident and outgoing evanescent wave modes with the same mode number (or the same $k_y^{(m)}$) value.

In the case of purely-propagating incident and scattered modes where the incident wave modes exist only on the left side of the disorder, a portion of the relation $(S_{parti}^{pr,pr})^\dagger S_{parti}^{pr,pr} = I$ leads to the well-known trace formula[10] for transmission and reflection averaged over different modes, $T_{pr} = (1/M_{pr}) Tr \left\{ (S_{21}^{pr,pr})^\dagger S_{21}^{pr,pr} \right\}$ and $R_{pr} = (1/M_{pr}) Tr \left\{ (S_{11}^{pr,pr})^\dagger S_{11}^{pr,pr} \right\}$ such that $T_{pr} + R_{pr} = 1$. Here, Tr stands for the trace of the matrix. For a purely evanescent incident wave, the scenario is different as the following. For the case of the incident evanescent wave modes (existing only on the left side of the disorder) and using the generalized unitarity relation $(S_{parti}^{pr,ev})^\dagger S_{parti}^{pr,ev} = i \left\{ (S_{parti}^{ev,ev})^\dagger - S_{parti}^{ev,ev} \right\}$,

$$\begin{aligned} & \frac{1}{M_{ev}} Tr \left\{ S_{21}^{pr,ev}^\dagger S_{21}^{pr,ev} \right\} + \frac{1}{M_{ev}} Tr \left\{ S_{11}^{pr,ev}^\dagger S_{11}^{pr,ev} \right\} \\ & = \frac{2}{M_{ev}} Im[Tr \{ S_{11}^{ev,ev} \}] \end{aligned} \quad (26)$$

This could be considered as the optical theorem for the Landauer-waveguide geometry involving the evanescent wave incidence, where the imaginary part of the sum of back-scattered evanescent reflection coefficients along the same direction of the incident evanescent modes, determine the outgoing propagating wave intensity. Next, the usefulness of the generalized S matrix components in the context of wavefront shaping is discussed.

V. FOCUSING OF AN EVANESCENT MODE AND UNIVERSAL BACKGROUND TRANSMISSION

This section covers the single mode focusing onto an evanescent mode by the phase conjugation of the transmitted propagating mode generated due to the same evanescent mode in a diffusive disorder. Let there be

a single evanescent mode (indexed by m') incident only from the right side onto the disorder. The incident evanescent mode gets transmitted as a propagating wave traveling to the left side of the disorder. The transmitted propagating wave on the left side can be represented as $c_{tr}^{L,pr} = S_{12}^{pr,ev} I_{m'}^{ev}$ where $I_{m'}^{ev}$ is a column vector to select the $(m')^{th}$ evanescent mode incidence. As an example $I_{m'=1}^{ev} = (1, 0, 0, \dots, 0)^T$, would select the first evanescent mode. The flux normalized phase conjugate of $c_{tr}^{L,pr}$ is then given as $c_1 (c_{tr}^{L,pr})^*$ which is incident on the left side of the disorder. Here, c_1 is used for the flux normalization and the value of c_1 is dependent on the $(m')^{th}$ evanescent mode used. The propagating phase conjugate wave incident from the left undergoes transmission on the right side to give

$$c_{tr}^{R,ev} = S_{21}^{ev,pr} \left\{ c_1 (S_{12}^{pr,ev})^* I_{m'}^{ev} \right\}, \quad (27a)$$

$$c_{tr}^{R,pr} = S_{21}^{pr,pr} \left\{ c_1 (S_{12}^{pr,ev})^* I_{m'}^{ev} \right\}. \quad (27b)$$

Here $c_{tr}^{R,ev}$ contains the complex coefficients for the evanescent component of the transmitted wave on the right side. Similarly, $c_{tr}^{R,pr}$ contains the propagating component forming the transmitting background. Substituting the reciprocity property (discussed in Sec. IV) that $S_{12}^{pr,ev} = i (S_{21}^{ev,pr})^T$ into Eq. 27a,

$$c_{tr}^{R,ev} = -i c_1 S_{21}^{ev,pr} (S_{21}^{ev,pr})^\dagger I_{m'} \quad (28)$$

In Eq. 28, the transmitted wave field peaks at the $(m')^{th}$ evanescent mode resulting in the constructive inference leading to focusing as expected and known. Such a focussing scenario is shown in FIG. 4 where the focussing onto a propagating and evanescent mode are done separately.

For the remaining part of the paper, we discuss about the optimal transmission due to the background propagating wave formed during the evanescent wave focusing. Such an optimal background transmission is defined as $T_{opt} = (c_{tr}^{R,pr})^\dagger c_{tr}^{R,pr}$ where $c_{tr}^{R,pr}$ is given in Eq. 27b. For diffusive disorders, ensemble averaged background transmission $\langle T_{opt} \rangle$ is observed to be 2/3 similar to that of the case of the focusing[29] of propagating modes. Such a phenomenon can be justified as the following for diffusive disorders.

The transmitted propagating mode $c_{tr}^{L,pr}$ on the left defined before, due to an incident evanescent mode on the right, could also be generated by an equivalent incident propagating mode as the following,

$$c_{tr}^{L,pr} = S_{12}^{pr,ev} I_{m'}^{ev} = c_0 S_{12}^{pr,pr} b_{12,m'}^{pr}, \quad (29)$$

where the incident propagating column vector $b_{12,m'}^{pr}$ is flux normalized as $(b_{12,m'}^{pr})^\dagger b_{12,m'}^{pr} = 1$ and c_0 is the coefficient satisfying Eq. 29 whose value depends on m' . In other words, the transmitted propagating wave after the disorder can be considered indistinguishable whether it

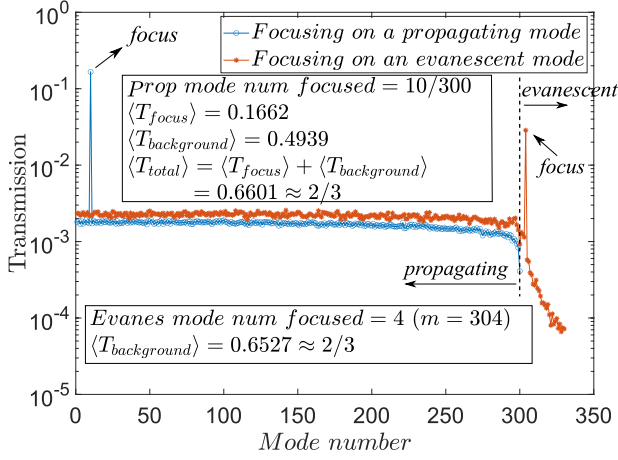


FIG. 4. **Ensemble averaged transmission while focusing via phase conjugation for a collection of cascaded disorders with $\langle \tau_{21}^{pr,pr} \rangle = 0.1489$.** Ensemble averaged (involving 1000 disordered slabs) distribution of transmission values while focusing onto a propagating mode and an evanescent mode in two separate focusing scenarios. The optimal transmission $\langle T_{opt} \rangle$ for the focusing of propagating mode is $\langle T_{total} \rangle = \langle T_{focus} \rangle + \langle T_{background} \rangle = 0.6603 \approx 2/3$, which is a universal constant[29] as expected. Here, $\langle \dots \rangle$ denotes averaging over ensemble. T_{focus} is the transmission only due to the focused mode and $T_{background}$ the total transmission summed over all the modes other than the focus. For the focusing of the evanescent mode, $\langle T_{opt} \rangle$ is the background transmission $T_{background}$ which is a universal constant such that $T_{background} = 0.6535 \approx 2/3$. The ensemble of generalized S matrices is generated by the S matrix cascading method explained in the supplementary Sec. VIII and in the user manual.

is generated by a single evanescent mode or by an equivalent propagating wave represented by $c_0 b_{12,m'}^{pr}$. This equivalent propagating wave yielding the same transmitted propagating wave due to the given evanescent mode, will be a linear combination of the propagating modes addressed by the propagating transmission matrix. Substituting Eq. 29 in Eq. 27b and using the reciprocity relation that $(S_{12}^{pr,pr})^* = S_{21}^{pr,pr \dagger}$,

$$\begin{aligned}
 T_{opt} &= c_{tr}^{R,pr \dagger} c_{tr}^{R,pr} = \\
 &c_0^2 c_1^2 \left(b_{12,m'}^{pr} \right)^T S_{21}^{pr,pr} \left(S_{21}^{pr,pr} \right)^\dagger S_{21}^{pr,pr} \left(S_{21}^{pr,pr} \right)^\dagger \left(b_{12,m'}^{pr} \right)^* \\
 &= c_0^2 c_1^2 \left(b_{12,m'}^{pr} \right)^T U_{21}^{pr,pr} \left(\tau_{21}^{pr,pr} \right)^2 U_{21}^{pr,pr \dagger} \left(b_{12,m'}^{pr} \right)^*, \quad (30)
 \end{aligned}$$

where the definition of the singular value decomposition of $S_{21}^{pr,pr} = U_{21}^{pr,pr} \sqrt{\tau_{21}^{pr,pr}} V_{21}^{pr,pr \dagger}$ is made use of. Here, $\tau_{21}^{pr,pr}$ is the diagonal matrix containing the eigenchannel transmission coefficients. Next, the ensemble-averaging of T_{opt} , denoted as $\langle T_{opt} \rangle$, is evaluated. For ensemble averaging, the isotropy[30, 31] assumption is made use of. Isotropy assumption considers that $(\tau_{21}^{pr,pr})^2$ and the

remaining terms in Eq. 30 are statistically uncorrelated from each other, while performing ensemble averaging. As τ_{21} obeys the bimodal distribution for diffusive media, $\langle T_{opt} \rangle$ has the universal value of $2/3$ similar to that of the focusing[29] of propagating modes. The associated proof involving the averaging over unitary groups is provided in the Appendix Sec. B. The relation $\langle T_{opt} \rangle = 2/3$ for the evanescent mode focusing is also numerically validated using the developed code as shown in the FIG. 4. Here, the ensemble averaging is performed by generating an ensemble of S matrices using the S matrix cascading method[32] (refer the supplementary Sec. VIII) by randomly shuffling the order of cascading. One may refer to the user manual for further details on the numerical validation.

VI. CONCLUSION

The analytical description and the associated numerical modeling to estimate the generalized S matrix is described from the point of view of the classical wave scattering for the Landauer-waveguide geometry. Although the Landauer-waveguide geometry is mostly used in the context of quantum transport, the classical wave scattering methods are used intentionally in this paper so that researchers coming from the engineering domain feel it easier to explore the mesoscopic wave transport theory. The authors believe that the presented method brings analytical tractability and generality with the help of Green's functions, even though the Green's function perturbation method by itself is not the most memory efficient computational method among the classes of algorithms available for estimating the S matrix. One may refer the recently published paper by Lin et al.[33] for a numerically efficient strategy for the S matrix estimation. The reduced memory efficiency with the Green's function method is circumvented in this paper by incorporating the S matrix cascading method. In the S matrix cascading method, the generalized S matrices of thinner layers were cascaded to obtain the effective S matrix of the thicker layer formed by the cascading of the thinner layers. Hence, the analysis for a thicker sample can be broken down into a cascade of thinner samples overcoming the computational burden of solving a large problem at once. Similarly, shuffling the order of S matrices while cascading could easily be used to generate ensembles of disorder for estimating various averages. As the Green's function perturbation method is used, starting from the analytical expression for the free-space Green's function involving a truncated number of evanescent modes, precise numerical control over the evanescent modes under consideration can be obtained.

Finally and most importantly, the usefulness of the model in wavefront shaping applications involving the focusing of an evanescent mode is demonstrated. The universal background transmission due to the focusing of evanescent modes is discussed. The authors believe that

these results and the associated code may be of interest to wavefront shaping researchers studying the transport aspects in general.

CODE REPOSITORY

The open source (MIT license) MATLAB[®] codes[34] used for modeling the results are hosted in Github <https://github.com/michaelraju/Generalized-S-Matrix>. The same repository is also hosted in Zenodo at <https://doi.org/10.5281/zenodo.10963078>. The saved run data associated with the code packages are also hosted at <https://doi.org/10.5281/zenodo.10960970>. One may download the saved run data from Zenodo and place it appropriately within the Github local repository to regenerate all the presented results without performing a new computational run from the scratch. One could also perform a new computational run initializing a new disorder by setting the appropriate flag mentioned in the user manual. One may refer to the user manual contained in the repository for the detailed description on the file structure of the associated code packages and how to use it. The computational simulation were performed on a desktop PC with a configuration of 64 GB of RAM and an eight-core processor.

AUTHOR CONTRIBUTIONS

M.R. derived the analytical and numerical description of the methodologies presented, and developed the associated simulation code packages. B.J. and S.A.E. were involved in the PhD supervision of the project. All authors were involved in the discussion, validation and interpretation of the results. M.R. wrote the manuscript and the supplementary documents with the support from other authors.

ACKNOWLEDGMENTS

We would like to thank Science Foundation Ireland (SFI) for funding the research through S.A.E's professorship grant "Novel applications and techniques for in-vivo optical imaging and spectroscopy" (SFI/15/RP/2828 and SFI/22/RP-2TF/10293).

Appendix A: Disorder properties

Supplementary Sec. I describes the numerical method adopted to generate the spatially correlated (but uniformly distributed) diffusive disorder as shown in FIG. 5. Such a disorder is used for estimating the generalized S matrix given in this paper.

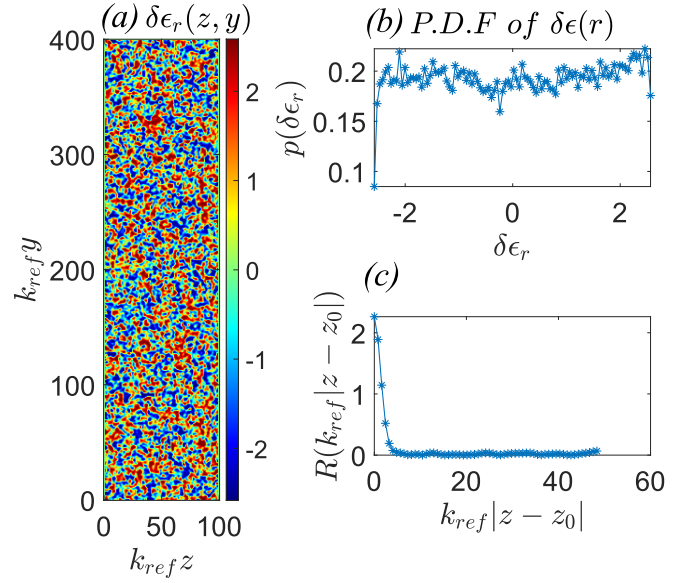


FIG. 5. **Spatially correlated and uniformly distributed disorder.** (a) Spatially correlated disorder, represented by the dielectric-constant perturbation $\delta\epsilon_r(z, y)$, modeled as per the Supplementary Sec. I A. (b) Probability density function of the disorder $\delta\epsilon_r(z, y)$ matrix elements such that the $\text{var}(\delta\epsilon_r) = 2.26$. (c) Spatial correlation function $R(k_{ref}|z - z_0|)$, defined in Eq. 1 of Supplementary Sec. I A, is plotted where the dimensionless spatial correlation length $k_{ref}l_c$ along z axis, is 2.01.

Appendix B: Proof that $\langle T_{opt} \rangle = 2/3$ for evanescent wave focusing

The goal of this section is to prove that for diffusive disorders, the ensemble average of T_{opt} given in Eq. 30,

$$\begin{aligned} \langle T_{opt} \rangle &= \langle c_0^2 c_1^2 \left(b_{12, m'}^{pr} \right)^T U_{21}^{pr, pr} (\tau_{21}^{pr, pr})^2 U_{21}^{pr, pr \dagger} \left(b_{12, m'}^{pr} \right)^* \rangle \\ &= 2/3. \end{aligned} \quad (\text{B1})$$

Using summation indices, the above equation can also be represented as

$$\begin{aligned} \langle T_{opt} \rangle &= \langle c_1^2 c_0^2 \sum_{m_1} \sum_{m_2} \sum_{m_3} \left\{ b_{12, m'}^{pr} \right\}_{m_1, 1} \left\{ b_{12, m'}^{pr} \right\}_{m_3, 1}^* \times \\ &\quad \left\{ U_{21}^{pr, pr} \right\}_{m_1, m_2} \left\{ (U_{21}^{pr, pr})^* \right\}_{m_3, m_2} \left\{ (\tau_{21}^{pr, pr})^2 \right\}_{m_2, m_2} \rangle \end{aligned} \quad (\text{B2})$$

Taking the isotropy assumption

$$\begin{aligned} \langle T_{opt} \rangle &= \langle c_1^2 c_0^2 \sum_{m_1} \sum_{m_2} \sum_{m_3} \langle \left\{ b_{12, m'}^{pr} \right\}_{m_1, 1} \left\{ b_{12, m'}^{pr} \right\}_{m_3, 1}^* \rangle \times \\ &\quad \langle \left\{ U_{21}^{pr, pr} \right\}_{m_1, m_2} \left\{ (U_{21}^{pr, pr})^* \right\}_{m_3, m_2} \left\{ (\tau_{21}^{pr, pr})^2 \right\}_{m_2, m_2} \rangle \end{aligned} \quad (\text{B3})$$

As per Sec. 3 of [30], $Q_{b\beta}^{\alpha\alpha} = \langle U_{b\beta} (U_{\alpha\alpha})^* \rangle = \delta_{ab} \delta_{\alpha\beta} / M_{pr}$ where δ is the Kronecker delta function and denoting $\sum_{m_2} \left\{ (\tau_{21}^{pr, pr})^2 \right\}_{m_2, m_2} = T_2$, $\langle T_{opt} \rangle$ can be simplified as,

$$\begin{aligned} \langle T_{opt} \rangle &= \langle c_1^2 c_0^2 \sum_{m_1} \sum_{m_3} \langle \left\{ b_{12, m'}^{pr} \right\}_{m_1, 1} \left\{ b_{12, m'}^{pr} \right\}_{m_3, 1}^* \rangle \times \\ &\quad (\delta_{m_1, m_3} / M_{pr}) \langle T_2 \rangle \end{aligned} \quad (\text{B4})$$

As $(b_{12,m'}^{pr})^\dagger b_{12,m'}^{pr} = 1$, $\langle T_{opt} \rangle$ is simplified as

$$\langle T_{opt} \rangle = \langle c_1^2 c_0^2 \rangle \langle T_2 \rangle / M_{pr} \quad (B5)$$

It can be shown (given towards the end of this section) that $\langle c_1^2 c_0^2 \rangle = 1/\langle \tau_{avg} \rangle$ where τ_{avg} is the numerical average of the eigenchannel transmission coefficients contained in the diagonal of the matrix $\tau_{21}^{pr,pr}$. For the bimodal eigenchannel transmission coefficient distribution, $\langle T_2 \rangle = 2g/3$ where $g = M_{pr} \langle \tau_{avg} \rangle$ is the optical conductance. Substituting these relations in Eq. B5, we get $\langle T_{opt} \rangle = 2/3$ which is a universal constant.

For the completeness of the proof, $\langle c_1^2 c_0^2 \rangle = 1/\langle \tau_{avg} \rangle$ is derived as the following. As given in the first paragraph of Sec. V, the flux normalized propagating phase conjugate wave incident on the left side of the disorder to create an evanescent focus on the right is represented as $c_1 (c_{tr}^{L,pr})^* = c_1 (S_{12}^{pr,ev})^* I_{m'}^{ev}$. But, it was seen that $(S_{12}^{pr,ev})^* I_{m'}^{ev} = c_0 (S_{12}^{pr,pr})^* (b_{12,m'}^{pr})^*$. As flux conservation implies $(c_1 (c_{tr}^{L,pr})^*)^\dagger (c_1 (c_{tr}^{L,pr})^*) = 1$, it leads to

$$c_1^2 c_0^2 (b_{12,m'}^{pr})^T (S_{12}^{pr,pr})^T (S_{12}^{pr,pr})^* (b_{12,m'}^{pr})^* = 1 \quad (B6)$$

Using the reciprocity relation that $(S_{12}^{pr,pr})^T (S_{12}^{pr,pr})^* =$

$S_{21}^{pr,pr} S_{21}^{pr,pr\dagger}$ and implementing the *S.V.D* of $S_{21}^{pr,pr}$,

$$c_1^2 c_0^2 (b_{12,m'}^{pr})^T U_{21}^{pr,pr} \tau_{21}^{pr,pr} (U_{21}^{pr,pr})^\dagger (b_{12,m'}^{pr})^* = 1 \quad (B7)$$

Taking the ensemble averaging with the isotropy assumption and using the summation indices,

$$\langle c_1^2 c_0^2 \rangle \sum_{m_3} \sum_{m_2} \sum_{m_1} \langle \{b_{12,m'}^{pr}\}_{m_1,1} \{b_{12,m'}^{pr}\}_{m_3,1}^* \rangle \times \langle \{U_{21}^{pr,pr}\}_{m_1,m_2} \{U_{21}^{pr,pr}\}_{m_3,m_2}^* \rangle \langle \{\tau_{21}^{pr,pr}\}_{m_2,m_2} \rangle = 1 \quad (B8)$$

Further simplifying, using the averaging over unitary groups,

$$\langle c_1^2 c_0^2 \rangle \sum_{m_3} \sum_{m_1} \langle \{b_{12,m'}^{pr}\}_{m_1,1} \{b_{12,m'}^{pr}\}_{m_3,1}^* \rangle \times (\delta_{m_1,m_3} / M_{pr}) \langle \sum_{m_2} \{\tau_{21}^{pr,pr}\}_{m_2,m_2} \rangle = 1. \quad (B9)$$

As $(b_{12,m'}^{pr})^\dagger b_{12,m'}^{pr} = 1$,

$$\langle c_1^2 c_0^2 \rangle (1/M_{pr}) (M_{pr} \langle \tau_{avg} \rangle) = 1. \quad (B10)$$

This results in the relation $\langle c_1^2 c_0^2 \rangle = 1/\langle \tau_{avg} \rangle$, which is used to simplify Eq. B5.

-
- [1] S. Rotter and S. Gigan, Light fields in complex media: Mesoscopic scattering meets wave control, *Reviews of Modern Physics* **89**, 015005 (2017).
- [2] I. M. Vellekoop and A. Mosk, Focusing coherent light through opaque strongly scattering media, *Optics letters* **32**, 2309 (2007).
- [3] S. Popoff, A. Goetschy, S. Liew, A. D. Stone, and H. Cao, Coherent control of total transmission of light through disordered media, *Physical review letters* **112**, 133903 (2014).
- [4] C. W. Hsu, S. F. Liew, A. Goetschy, H. Cao, and A. D. Stone, Correlation-enhanced control of wave focusing in disordered media, *Nature Physics* **13**, 497 (2017).
- [5] O. Katz, F. Ramaz, S. Gigan, and M. Fink, Controlling light in complex media beyond the acoustic diffraction-limit using the acousto-optic transmission matrix, *Nature communications* **10**, 1 (2019).
- [6] O. S. Ojambati, H. Yilmaz, A. Lagendijk, A. P. Mosk, and W. L. Vos, Coupling of energy into the fundamental diffusion mode of a complex nanophotonic medium, *New journal of physics* **18**, 043032 (2016).
- [7] R. Sarma, A. G. Yamilov, S. Petrenko, Y. Bromberg, and H. Cao, Control of energy density inside a disordered medium by coupling to open or closed channels, *Physical review letters* **117**, 086803 (2016).
- [8] N. Bender, A. Yamilov, A. Goetschy, H. Yilmaz, C. W. Hsu, and H. Cao, Depth-targeted energy delivery deep inside scattering media, *Nature Physics*, 1 (2022).
- [9] S. M. Popoff, G. Lerosey, R. Carminati, M. Fink, A. C. Boccara, and S. Gigan, Measuring the transmission matrix in optics: an approach to the study and control of light propagation in disordered media, *Physical review letters* **104**, 100601 (2010).
- [10] D. S. Fisher and P. A. Lee, Relation between conductivity and transmission matrix, *Physical Review B* **23**, 6851 (1981).
- [11] A. Goetschy and A. Stone, Filtering random matrices: the effect of incomplete channel control in multiple scattering, *Physical review letters* **111**, 063901 (2013).
- [12] H. Yilmaz, C. W. Hsu, A. Yamilov, and H. Cao, Transverse localization of transmission eigenchannels, *Nature Photonics* **13**, 352 (2019).
- [13] E. Akkermans and G. Montambaux, *Mesoscopic physics of electrons and photons* (Cambridge university press, 2007).
- [14] G. Lerosey, J. De Rosny, A. Tourin, and M. Fink, Focusing beyond the diffraction limit with far-field time reversal, *Science* **315**, 1120 (2007).
- [15] J. Park, C. Park, K. Lee, Y.-H. Cho, and Y. Park, Time-reversing a monochromatic subwavelength optical focus by optical phase conjugation of multiply-scattered light, *Scientific reports* **7**, 1 (2017).
- [16] R. Carminati, J. Saenz, J.-J. Greffet, and M. Nieto-Vesperinas, Reciprocity, unitarity, and time-reversal symmetry of the s matrix of fields containing evanescent components, *Physical review A* **62**, 012712 (2000).
- [17] M. Davy, Z. Shi, and A. Z. Genack, Focusing through random media: Eigenchannel participation number and intensity correlation, *Physical Review B* **85**, 035105 (2012).
- [18] M. Raju, B. Jayet, and S. Andersson-Engels, Supplementary material : Modeling scattering matrix containing evanescent modes for wavefront shaping applications in disordered media, URL_will_be_inserted_by_publisher.
- [19] J. Schmitt and G. Kumar, Turbulent nature of refractive-index variations in biological tissue, *Optics letters* **21**,

- 1310 (1996).
- [20] L. B. Felsen, F. Akleman, and L. Sevgi, Wave propagation inside a two-dimensional perfectly conducting parallel-plate waveguide: Hybrid ray-mode techniques and their visualizations, *IEEE Antennas and Propagation Magazine* **46**, 69 (2004).
- [21] R. Carminati and J. C. Schotland, *Principles of Scattering and Transport of Light* (Cambridge University Press, 2021).
- [22] O. J. Martin, A. Dereux, and C. Girard, Iterative scheme for computing exactly the total field propagating in dielectric structures of arbitrary shape, *JOSA A* **11**, 1073 (1994).
- [23] O. J. Martin, C. Girard, and A. Dereux, Generalized field propagator for electromagnetic scattering and light confinement, *Physical Review Letters* **74**, 526 (1995).
- [24] P. Dömötör, P. Földi, M. G. Benedict, B. W. Shore, and W. P. Schleich, Scattering of a particle with internal structure from a single slit: exact numerical solutions, *New Journal of Physics* **17**, 023044 (2015).
- [25] S. Datta, *Electronic transport in mesoscopic systems* (Cambridge university press, 1997).
- [26] N. Byrnes and M. R. Foreman, Symmetry constraints for vector scattering and transfer matrices containing evanescent components: Energy conservation, reciprocity, and time reversal, *Physical Review Research* **3**, 013129 (2021).
- [27] Y. V. Gulyaev, Y. N. Barabanenkov, M. Y. Barabanenkov, and S. Nikitov, Optical theorem for electromagnetic field scattering by dielectric structures and energy emission from the evanescent wave, *Physical Review E* **72**, 026602 (2005).
- [28] M. Y. Barabanenkov, Y. N. Barabanenkov, Y. V. Gulyaev, and S. Nikitov, Energy emission from evanescent wave and interference of opposite wave streams, *Physics Letters A* **364**, 421 (2007).
- [29] I. M. Vellekoop and A. Mosk, Universal optimal transmission of light through disordered materials, *Physical review letters* **101**, 120601 (2008).
- [30] P. Mello, Averages on the unitary group and applications to the problem of disordered conductors, *Journal of Physics A: Mathematical and General* **23**, 4061 (1990).
- [31] P. A. Mello and A. D. Stone, Maximum-entropy model for quantum-mechanical interference effects in metallic conductors, *Physical Review B* **44**, 3559 (1991).
- [32] C. Jin, *New Methods and Theory for Increasing Transmission of Light through Highly-Scattering Random Media.*, Ph.D. thesis (2014).
- [33] H.-C. Lin, Z. Wang, and C. W. Hsu, Fast multi-source nanophotonic simulations using augmented partial factorization, *Nature Computational Science* **2**, 815 (2022).
- [34] M. Raju, B. Jayet, and S. Andersson-Engels, Matlab code packages for Modeling scattering matrix containing evanescent modes for wavefront shaping applications in disordered media 10.5281/zenodo.10963078 (2024).

Supplementary Material : Modeling scattering matrix containing evanescent modes for wavefront shaping applications in disordered media

Michael Raju,^{1,2,*} Baptiste Jayet,¹ and Stefan Andersson-Engels^{1,2}

¹ Tyndall National Institute, Lee Maltings Complex, Dyke Parade, Cork, Ireland, T12 R5CP

² School of Physics, University College Cork, College Road, Cork, Ireland, T12 K8AF

I. SPATIALLY CORRELATED DISORDERS

If the random disorder ensemble (characterized by its spatial refractive index fluctuations) drawn from a particular probability distribution is considered as a spatial random process, then according to the Wiener–Khinchin theorem, the randomness power spectrum of the disorder can be estimated by the spatial Fourier transform of its correlation function. Therefore, to create a random disorder with a particular correlation length, either the spatial correlation function (in real space) or the randomness power spectrum (in the spatial Fourier space) could be used. Here, we use the Fourier space method (as described in the Supplementary Sec. IA), for generating a uniformly-distributed Gaussian-correlated disorder. The disorder is represented in terms of the spatial dielectric-constant perturbation $\delta\tilde{\epsilon}_r(z, y)$ defined such that it is uniformly distributed with zero-mean and has a Gaussian spatial correlation. To characterize the disorder, variance is defined as $var_{disorder} = \langle \delta\tilde{\epsilon}_r(r)^2 \rangle - \langle \delta\tilde{\epsilon}_r(r) \rangle^2 = \langle \delta\tilde{\epsilon}_r(r)^2 \rangle$. The spatial correlation function can be defined as $R(k_{ref}r, k_{ref}r_0) = \langle \delta\tilde{\epsilon}_r(k_{ref}z, k_{ref}y) \delta\tilde{\epsilon}_r(k_{ref}z_0, k_{ref}y_0) \rangle$, where $R(k_{ref}r, k_{ref}r_0)$ is the un-normalized spatial correlation function. For a statistically homogeneous disorder, $R(k_{ref}r, k_{ref}r_0) = R(k_{ref}|r - r_0|)$. It can be noted from the definition of the disorder variance that $R(k_{ref}r_0, k_{ref}r_0) = R(0) = var_{disorder}$. Therefore, to represent the un-normalized spatial correlation function of the disorder, $R(0)$ value can be combined with a normalized correlation function $C_{disorder}(k_{ref}|r - r_0|)$ as given below

$$R(k_{ref}|r - r_0|) = R(0)C_{disorder}(k_{ref}|r - r_0|), \quad (1)$$

where the normalized two-point Gaussian spatial correlation function, $C_{disorder}(k_{ref}|r - r_0|)$ for $\delta\tilde{\epsilon}_r(r)$ as the following

$$C_{disorder}(k_{ref}|r - r_0|) = e^{-(k_{ref}|r - r_0|)^2 / (k_{ref}^2 l_c^2)} \quad (2)$$

The power spectral density of the disorder ($P_{PSD}(p_z, p_y)$) is defined as the Fourier transform (\mathcal{F}) of the spatial correlation function.

$$P_{PSD}(p_z, p_y) = \mathcal{F} \{ R(k_{ref}|r - r_0|) \} = var_{disorder} \mathcal{F} \{ C_{disorder}(r, l_c) \} \quad (3)$$

where p_z and p_y are angular spatial frequencies. Having reviewed the essential concepts, using the numerical algorithm given in supplementary Sec. IA, a uniformly distributed-spatially correlated disorder is modeled.

A. Method for generating uniformly-distributed spatially-correlated disorder

The steps for estimating the uniformly-distributed Gaussian-correlated disorder are given as the following.

1. Estimate $\delta\epsilon_{\text{fft}}^{white} = \text{fft2}(\delta\epsilon_r^{white}(z, y))$ where fft2 is the two dimensional Fourier transform and $\delta\epsilon_r^{white}(z, y)$ is the white-noise like uncorrelated disorder generated from a uniform probability distribution.
2. Take an element-wise product in the Fourier space to obtain $\delta\epsilon_{\text{fft}}^{corr} = \delta\epsilon_{\text{fft}}^{white} \mathcal{F} \{ C_{disorder}(r, l_c) \}$
3. Apply inverse Fourier transform to estimate the correlated disorder in the real space with spatial correlation length l_c , given by $\delta\epsilon_r^{corr}(z, y) = \text{ifft2}(\delta\epsilon_{\text{fft}}^{corr})$ where ifft2 is the two dimensional inverse Fourier transform.
4. Normalize $\delta\epsilon_r^{corr}(z, y)$ by dividing it with the standard deviation of the matrix elements. This results in a Gaussian distributed (with unit variance) and Gaussian correlated (with correlation length l_c) disorder.

* michaelraju@umail.ucc.ie

5. To transform the Gaussian distributed-Gaussian correlated disorder to a uniform distributed-Gaussian correlated disorder, a Gaussian cumulative probability distribution function (*C.D.F*) can be used. A zero mean Gaussian *C.D.F* takes a normally distributed random variable and converts it into a transformed random variable between (0, 1) giving a uniform distribution. Hence, every matrix element of Gaussian distributed-Gaussian correlated disorder can be transformed between (0, 1) using the Gaussian *C.D.F*. Such a uniformly distributed disorder between (0, 1) can then be scaled between $\min \{\delta\epsilon^{white}\}$ and $\max \{\delta\epsilon^{white}\}$ to have similar spread in values with that of the uncorrelated white-noise like disorder.
6. Real space spatial correlation of the obtained disorder can be numerically estimated and validated against the l_c value used for defining the correlation function by the following method. It involves the Fourier space method for evaluating spatial autocorrelation of a 2D matrix. For an $M \times N$ correlated disorder $\delta\epsilon_r^{corr}(z, y)$,

$$R_{disorder}(k_{ref}|r - r_0|) = |\text{ifft2}[\text{fft2}(\delta\epsilon_r^{corr})(\text{fft2}(\delta\epsilon_r^{corr}))^*]|/(MN) \quad (4)$$

where * denotes complex conjugation. Numerically estimated correlation length can be defined as the length at which the correlation function decays from $R(0)$ to $R(0)/e$.

II. ESTIMATING THE PERTURBED GREEN'S FUNCTION $G(r, r_0)$

The discretized Dyson's equation in 2D is $G_{ij} = G_{ij}^{(0)} + \sum_{k=1}^{N_z^P N_y^P} G_{ik}^{(0)} V_k \Delta_{area} G_{kj}$ where k is used as a index. The entire computational domain which includes the disordered perturbation region and the surrounding region for field visualization, has the size of $[N_y \times N_z]$. The disorder perturbation region has the size of $[N_y^P \times N_z^P]$, which is a subset of the computational domain $[N_y \times N_z]$. Therefore, there are $N_z^P N_y^P$ scatterer perturbation points. Here, the index i denotes the field evaluation location accessed linearly as a 1D array. Similarly, the index j denotes the source location accessed linearly as a 1D array, placed on the boundaries Γ_L or Γ_R . The index k accessed linearly as a 1D array, is associated with the locations at which the scatterer perturbation exists. Two methods are presented as the following where the first method is the direct matrix inversion method. Such a method is easier to understand, but it is memory intensive. The second method is the iterative method which requires iteration steps, but it is memory efficient.

Both the methods start by estimating the free space Green's function $G_{ik}^{(0)}$ and $G_{ij}^{(0)}$, where i spans all the field evaluation points of size $N_y N_z$ for visualisation purposes, k spans all the $N_z^P N_y^P$ scatterer position points where the perturbation is about to be brought in, and j the N_y points associated with the left or the right boundary. $G_{ik}^{(0)}$ is of the dimension $[N_y N_z \times N_y^P N_z^P]$. Other Green's function terms to be appearing in the methods can be derived as a subset from $G_{ik}^{(0)}$ and $G_{ij}^{(0)}$.

A. Direct method

Step 1 : Using the Dyson's equation, solve for G_{kj} for different locations of $k = k_1, k_2, k_3, \dots, k_{N_z^P N_y^P}$ and a given j location

$$G_{k_1 j} = G_{k_1 j}^{(0)} + \begin{bmatrix} G_{k_1 k_1}^{(0)} V_{k_1} & G_{k_1 k_2}^{(0)} V_{k_2} & \dots & G_{k_1 k_{N_z^P N_y^P}}^{(0)} V_{k_{N_z^P N_y^P}} \end{bmatrix} \begin{pmatrix} \Delta_{area} G_{k_1 j} \\ \Delta_{area} G_{k_2 j} \\ \dots \\ \Delta_{area} G_{k_{(N_z^P N_y^P)} j} \end{pmatrix} \quad (5)$$

$$G_{k_2 j} = G_{k_2 j}^{(0)} + \begin{bmatrix} G_{k_2 k_1}^{(0)} V_{k_1} & G_{k_2 k_2}^{(0)} V_{k_2} & \dots & G_{k_2 k_{N_z^P N_y^P}}^{(0)} V_{k_{N_z^P N_y^P}} \end{bmatrix} \begin{pmatrix} \Delta_{area} G_{k_1 j} \\ \Delta_{area} G_{k_2 j} \\ \dots \\ \Delta_{area} G_{k_{(N_z^P N_y^P)} j} \end{pmatrix} \quad (6)$$

⋮

$$G_{k_{(N_z^P N_y^P)} j} = G_{k_{(N_z^P N_y^P)} j}^{(0)} + \begin{bmatrix} G_{k_{(N_z^P N_y^P)} k_1}^{(0)} V_{k_1} & G_{k_{(N_z^P N_y^P)} k_2}^{(0)} V_{k_2} \dots & G_{k_{(N_z^P N_y^P)} k_{N_z^P N_y^P}}^{(0)} V_{k_{N_z^P N_y^P}} \end{bmatrix} \begin{pmatrix} \Delta_{area} G_{k_1 j} \\ \Delta_{area} G_{k_2 j} \\ \dots \\ \Delta_{area} G_{k_{(N_z^P N_y^P)} j} \end{pmatrix} \quad (7)$$

These set of equations can be written in a matrix form as

$$\begin{pmatrix} G_{k_1j} \\ G_{k_2j} \\ G_{k_3j} \\ \vdots \\ G_{k_{(N_z^P N_y^P)}j} \end{pmatrix} = \begin{pmatrix} G_{k_1j}^{(0)} \\ G_{k_2j}^{(0)} \\ G_{k_3j}^{(0)} \\ \vdots \\ G_{k_{(N_z^P N_y^P)}j}^{(0)} \end{pmatrix} + \underbrace{\begin{pmatrix} G_{k_1k_1}^{(0)} V_{k_1} & G_{k_1k_2}^{(0)} V_{k_2} & \cdots & G_{k_1k_{(N_z^P N_y^P)}}^{(0)} V_{k_{(N_z^P N_y^P)}} \\ G_{k_2k_1}^{(0)} V_{k_1} & G_{k_2k_2}^{(0)} V_{k_2} & \cdots & G_{k_2k_{(N_z^P N_y^P)}}^{(0)} V_{k_{(N_z^P N_y^P)}} \\ G_{k_3k_1}^{(0)} V_{k_1} & G_{k_3k_2}^{(0)} V_{k_2} & \cdots & G_{k_3k_{(N_z^P N_y^P)}}^{(0)} V_{k_{(N_z^P N_y^P)}} \\ \vdots & \vdots & \vdots & \vdots \\ G_{k_{(N_z^P N_y^P)}k_1}^{(0)} V_{k_1} & G_{k_{(N_z^P N_y^P)}k_2}^{(0)} V_{k_2} & \cdots & G_{k_{(N_z^P N_y^P)}k_{(N_z^P N_y^P)}}^{(0)} V_{k_{(N_z^P N_y^P)}} \end{pmatrix} \begin{pmatrix} \Delta_{area} G_{k_1j} \\ \Delta_{area} G_{k_2j} \\ \Delta_{area} G_{k_3j} \\ \vdots \\ \Delta_{area} G_{k_{(N_z^P N_y^P)}j} \end{pmatrix} \quad (8)$$

Representing the same system of equations as a matrix equation, G_{kj} is solved involving an M matrix (M matrix defined in the above given equation), as given below

$$\begin{aligned} [G_{kj}] &= [G_{kj}^{(0)}] + [M] [G_{kj}] \implies \\ [G_{kj}] &= [I - [M]]^{-1} [G_{kj}^{(0)}] \end{aligned} \quad (9)$$

Step 2 : Once $[G_{kj}]$ is obtained, evaluate $[G_{ij}]$ for a given j

$$\begin{pmatrix} G_{i_1j} \\ G_{i_2j} \\ G_{i_3j} \\ \vdots \\ G_{i_{(N_z N_y)}j} \end{pmatrix} = \begin{pmatrix} G_{i_1j}^{(0)} \\ G_{i_2j}^{(0)} \\ G_{i_3j}^{(0)} \\ \vdots \\ G_{i_{(N_z N_y)}j}^{(0)} \end{pmatrix} + \begin{pmatrix} G_{i_1k_1}^{(0)} V_{k_1} & G_{i_1k_2}^{(0)} V_{k_2} & \cdots & G_{i_1k_{(N_z^P N_y^P)}}^{(0)} V_{k_{(N_z^P N_y^P)}} \\ G_{i_2k_1}^{(0)} V_{k_1} & G_{i_2k_2}^{(0)} V_{k_2} & \cdots & G_{i_2k_{(N_z^P N_y^P)}}^{(0)} V_{k_{(N_z^P N_y^P)}} \\ G_{i_3k_1}^{(0)} V_{k_1} & G_{i_3k_2}^{(0)} V_{k_2} & \cdots & G_{i_3k_{(N_z^P N_y^P)}}^{(0)} V_{k_{(N_z^P N_y^P)}} \\ \vdots & \vdots & \vdots & \vdots \\ G_{i_{(N_z N_y)}k_1}^{(0)} V_{k_1} & G_{i_{(N_z N_y)}k_2}^{(0)} V_{k_2} & \cdots & G_{i_{(N_z N_y)}k_{(N_z^P N_y^P)}}^{(0)} V_{k_{(N_z^P N_y^P)}} \end{pmatrix} \begin{pmatrix} \Delta_{area} G_{k_1j} \\ \Delta_{area} G_{k_2j} \\ \Delta_{area} G_{k_3j} \\ \vdots \\ \Delta_{area} G_{k_{(N_z^P N_y^P)}j} \end{pmatrix} \quad (10)$$

where there is $N_z N_y$ field evaluation points due to $N_z^P N_y^P$ scattering particles. With step 1 and step 2 evaluated for different source locations j , G_{ij} can be fully solved. Although the direct method presented in this subsection is short and easy to understand, it is memory intensive because of the formation of the large non-sparse M matrix (of size $N_z^P N_y^P \times N_z^P N_y^P$) and the associated inversion process in the Eq. 9. Also, the free space Green's function $G_{ik}^{(0)}$ needs to be evaluated for the i corresponding to the entire $[N_z \times N_y]$ grid for the purpose of visualization. The location k needs to be spanned through all the scattering particle locations (to evaluate the M matrix), consuming memory. To save memory the following iterative method is used instead.

B. Iterative method involving slices of scatterers

In the iterative method, the total scattering block is divided into slices and the Green's function is updated accounting the scattering effect of the slices taken one at a time. As an example, let's say the entire scattering region

is divided into 10 slices. $G_{ik}^{(0)}$ needs to be evaluated like before for the source k location spanning all the particle positions. $G_{ij}^{(0)}$ is also evaluated where j is on Γ_L or Γ_R . Accounting the scattering perturbation of slice number 1 yields the new updated Green's function $G_{ik}^{(1)}$. While evaluating $G_{ik}^{(1)}$, the source k locations needs to be only those scatterer positions where the remaining 9 slices are to be brought in and also on the boundaries. One could overwrite the $G_{ik}^{(0)}$ array data (only for the source locations of the particles to be brought in, corresponding to the remaining 9 slices) for saving memory. Now the second slice is brought in and $G_{ik}^{(1)}$ is used to evaluate $G_{ik}^{(2)}$ accounting the scattering effect of the second slice. For evaluating $G_{ik}^{(2)}$, the source k locations needs to be only those scatterer locations where the remaining 8 slices are to be brought in and also on the boundaries. The method is repeated by bringing in the remaining slices one by one and updating the Green's function by overwriting the previous version, for the remaining particle positions. Therefore, the process becomes faster upon progressing through the slices.

First, let the first transverse slice of the scatterers be chosen, numbered 1 : N_y^P denoted as $1 \rightarrow N_y^P$. Solve the Eq. 8 just for the first slice.

Main step 1 for the iteration method involving the first slice of scatterers

• *Sub-step 1:*

$$\begin{pmatrix} G_{k_1 j}^{(1)} \\ G_{k_2 j}^{(1)} \\ G_{k_3 j}^{(1)} \\ \vdots \\ G_{k_{(N_y^P)} j}^{(1)} \end{pmatrix} = \begin{pmatrix} G_{k_1 j}^{(0)} \\ G_{k_2 j}^{(0)} \\ G_{k_3 j}^{(0)} \\ \vdots \\ G_{k_{(N_y^P)} j}^{(0)} \end{pmatrix} + \underbrace{\begin{pmatrix} G_{k_1 k_1}^{(0)} V_{k_1} & G_{k_1 k_2}^{(0)} V_{k_2} & \cdots & G_{k_1 k_{(N_y^P)}}^{(0)} V_{k_{(N_y^P)}} \\ G_{k_2 k_1}^{(0)} V_{k_1} & G_{k_2 k_2}^{(0)} V_{k_2} & \cdots & G_{k_2 k_{(N_y^P)}}^{(0)} V_{k_{(N_y^P)}} \\ G_{k_3 k_1}^{(0)} V_{k_1} & G_{k_3 k_2}^{(0)} V_{k_2} & \cdots & G_{k_3 k_{(N_y^P)}}^{(0)} V_{k_{(N_y^P)}} \\ \vdots & \vdots & \vdots & \vdots \\ G_{k_{(N_y^P)} k_1}^{(0)} V_{k_1} & G_{k_{(N_y^P)} k_2}^{(0)} V_{k_2} & \cdots & G_{k_{(N_y^P)} k_{(N_y^P)}}^{(0)} V_{k_{(N_y^P)}} \end{pmatrix}}_{M_{(1 \rightarrow N_y^P)}^{(0)}} \begin{pmatrix} \Delta_{area} G_{k_1 j}^{(1)} \\ \Delta_{area} G_{k_2 j}^{(1)} \\ \Delta_{area} G_{k_3 j}^{(1)} \\ \vdots \\ \Delta_{area} G_{k_{(N_y^P)} j}^{(1)} \end{pmatrix} \quad (11)$$

• *Sub-step 2:* Representing the above given system of equations as a matrix equation, $G_{k_{(1 \rightarrow N_y^P)} j}^{(1)}$ is solved involving the $M_{(1 \rightarrow N_y^P)}^{(0)}$ matrix (defined in the previous equation), as given below

$$\begin{aligned} \left[G_{k_{(1 \rightarrow N_y^P)} j}^{(1)} \right] &= \left[G_{k_{(1 \rightarrow N_y^P)} j}^{(0)} \right] + \left[M_{(1 \rightarrow N_y^P)}^{(0)} \right] \left[G_{k_{(1 \rightarrow N_y^P)} j}^{(1)} \right] \implies \\ \left[G_{k_{(1 \rightarrow N_y^P)} j}^{(1)} \right] &= \left[I - \left[M_{(1 \rightarrow N_y^P)}^{(0)} \right] \right]^{-1} \left[G_{k_{(1 \rightarrow N_y^P)} j}^{(0)} \right] \end{aligned} \quad (12)$$

• *Sub-step 3:* Once $[G_{k_{(1 \rightarrow N_y^P)} j}^{(1)}]$ is obtained, evaluate $[G_{ij}^{(1)}]$ for a given j

$$\begin{pmatrix} G_{i_1 j}^{(1)} \\ G_{i_2 j}^{(1)} \\ G_{i_3 j}^{(1)} \\ \vdots \\ G_{i_{(N_z N_y)} j}^{(1)} \end{pmatrix} = \begin{pmatrix} G_{i_1 j}^{(0)} \\ G_{i_2 j}^{(0)} \\ G_{i_3 j}^{(0)} \\ \vdots \\ G_{i_{(N_z N_y)} j}^{(0)} \end{pmatrix} + \begin{pmatrix} G_{i_1 k_1}^{(0)} V_{k_1} & G_{i_1 k_2}^{(0)} V_{k_2} & \cdots & G_{i_1 k_{(N_y^P)}}^{(0)} V_{k_{(N_y^P)}} \\ G_{i_2 k_1}^{(0)} V_{k_1} & G_{i_2 k_2}^{(0)} V_{k_2} & \cdots & G_{i_2 k_{(N_y^P)}}^{(0)} V_{k_{(N_y^P)}} \\ G_{i_3 k_1}^{(0)} V_{k_1} & G_{i_3 k_2}^{(0)} V_{k_2} & \cdots & G_{i_3 k_{(N_y^P)}}^{(0)} V_{k_{(N_y^P)}} \\ \vdots & \vdots & \vdots & \vdots \\ G_{i_{(N_z N_y)} k_1}^{(0)} V_{k_1} & G_{i_{(N_z N_y)} k_2}^{(0)} V_{k_2} & \cdots & G_{i_{(N_z N_y)} k_{(N_y^P)}}^{(0)} V_{k_{(N_y^P)}} \end{pmatrix} \begin{pmatrix} \Delta_{area} G_{k_1 j}^{(1)} \\ \Delta_{area} G_{k_2 j}^{(1)} \\ \Delta_{area} G_{k_3 j}^{(1)} \\ \vdots \\ \Delta_{area} G_{k_{(N_y^P)} j}^{(1)} \end{pmatrix} \quad (13)$$

• *Sub-step 4:* Before moving onto the next main iteration step (main iteration step number 2), the following sub-step evaluations has to be performed to estimate $[G_{k_{(1 \rightarrow N_y^P)} k_{(N_y^P+1 \rightarrow N_y^P N_z^P)}}^{(1)}]$ and $[G_{ik_{(N_y^P+1 \rightarrow N_y^P N_z^P)}}^{(1)}]$ to be used in the next main iteration step. Here $(N_y^P + 1 \rightarrow N_y^P N_z^P)$ corresponds to the remaining scatter position where the perturbation is brought-in in the future iteration steps by introducing slice number 2,3,4 etc..

Using Eq. 12,

$$\left[G_{k_{(1 \rightarrow N_y^P)} k_{(N_y^P+1 \rightarrow N_y^P N_z^P)}}^{(1)} \right] = \left[I - \left[M_{(1 \rightarrow N_y^P)}^{(0)} \right] \right]^{-1} \left[G_{k_{(1 \rightarrow N_y^P)} k_{(N_y^P+1 \rightarrow N_y^P N_z^P)}}^{(0)} \right] \quad (14)$$

Taking Eq. 13 and substituting for j as $k_{(N_y^p+1 \rightarrow N_y^p N_z^p)}$, together with the above given equation, $[G_{ik_{(N_y^p+1 \rightarrow N_y^p N_z^p)}}^{(1)}]$ can be estimated. The estimated $[G_{ik_{(N_y^p+1 \rightarrow N_y^p N_z^p)}}^{(1)}]$ can be overwritten upon the existing memory taken by $G_{ik}^{(0)}$.

Main step 2 involving the second slice of scatterers denoted by $N_y^p + 1 \rightarrow 2N_y^p$,

• *Sub-step 1:*

$$\begin{pmatrix} G_{k_{(N_y^p+1)j}}^{(2)} \\ G_{k_{(N_y^p+2)j}}^{(2)} \\ G_{k_{(N_y^p+3)j}}^{(2)} \\ \vdots \\ G_{k_{(2N_y^p)j}}^{(2)} \end{pmatrix} = \begin{pmatrix} G_{k_{(N_y^p+1)j}}^{(1)} \\ G_{k_{(N_y^p+2)j}}^{(1)} \\ G_{k_{(N_y^p+3)j}}^{(1)} \\ \vdots \\ G_{k_{(2N_y^p)j}}^{(1)} \end{pmatrix} + \underbrace{\begin{pmatrix} G_{k_{(N_y^p+1)k_{(N_y^p+1)}}^{(1)}} V_{k_{(N_y^p+1)}} & G_{k_{(N_y^p+1)k_{(N_y^p+2)}}^{(1)}} V_{k_{(N_y^p+2)}} & \cdots & G_{k_{(N_y^p+1)k_{(2N_y^p)}}^{(1)}} V_{k_{(2N_y^p)}} \\ G_{k_{(N_y^p+2)k_{(N_y^p+1)}}^{(1)}} V_{k_{(N_y^p+1)}} & G_{k_{(N_y^p+2)k_{(N_y^p+2)}}^{(1)}} V_{k_{(N_y^p+2)}} & \cdots & G_{k_{(N_y^p+2)k_{(2N_y^p)}}^{(1)}} V_{k_{(2N_y^p)}} \\ G_{k_{(N_y^p+3)k_{(N_y^p+1)}}^{(1)}} V_{k_{(N_y^p+1)}} & G_{k_{(N_y^p+3)k_{(N_y^p+2)}}^{(1)}} V_{k_{(N_y^p+2)}} & \cdots & G_{k_{(N_y^p+3)k_{(2N_y^p)}}^{(1)}} V_{k_{(2N_y^p)}} \\ \vdots & \vdots & \vdots & \vdots \\ G_{k_{(2N_y^p)k_{(N_y^p+1)}}^{(1)}} V_{k_{(N_y^p+1)}} & G_{k_{(2N_y^p)k_{(N_y^p+2)}}^{(1)}} V_{k_{(N_y^p+2)}} & \cdots & G_{k_{(2N_y^p)k_{(2N_y^p)}}^{(1)}} V_{k_{(2N_y^p)}} \end{pmatrix} \begin{pmatrix} \Delta_{area} G_{k_{(N_y^p+1)j}}^{(2)} \\ \Delta_{area} G_{k_{(N_y^p+2)j}}^{(2)} \\ \Delta_{area} G_{k_{(N_y^p+3)j}}^{(2)} \\ \vdots \\ \Delta_{area} G_{k_{(2N_y^p)j}}^{(2)} \end{pmatrix} \quad (15)$$

$M_{(N_y^p+1 \rightarrow 2N_y^p)}^{(1)}$

• *Sub-step 2:* Representing the above given system of equations as a matrix equation, $G_{k_{(N_y^p+1 \rightarrow 2N_y^p)j}}^{(2)}$ is solved involving the $M_{(N_y^p+1 \rightarrow 2N_y^p)}^{(1)}$ matrix (defined in the previous equation), as given below

$$\begin{aligned} \begin{bmatrix} G_{k_{(N_y^p+1 \rightarrow 2N_y^p)j}}^{(2)} \end{bmatrix} &= \begin{bmatrix} G_{k_{(N_y^p+1 \rightarrow 2N_y^p)j}}^{(1)} \end{bmatrix} + \begin{bmatrix} M_{(N_y^p+1 \rightarrow 2N_y^p)}^{(1)} \end{bmatrix} \begin{bmatrix} G_{k_{(N_y^p+1 \rightarrow 2N_y^p)j}}^{(2)} \end{bmatrix} \implies \\ \begin{bmatrix} G_{k_{(N_y^p+1 \rightarrow 2N_y^p)j}}^{(2)} \end{bmatrix} &= \left[I - \begin{bmatrix} M_{(N_y^p+1 \rightarrow 2N_y^p)}^{(1)} \end{bmatrix} \right]^{-1} \begin{bmatrix} G_{k_{(N_y^p+1 \rightarrow 2N_y^p)j}}^{(1)} \end{bmatrix} \end{aligned} \quad (16)$$

• *Sub-step 3:* Once $[G_{k_{(N_y^p+1 \rightarrow 2N_y^p)j}}^{(2)}]$ is obtained, evaluate $[G_{ij}^{(2)}]$ for a given j .

$$\begin{pmatrix} G_{i_1 j}^{(2)} \\ G_{i_2 j}^{(2)} \\ G_{i_3 j}^{(2)} \\ \vdots \\ G_{i_{(N_z N_y)} j}^{(2)} \end{pmatrix} = \begin{pmatrix} G_{i_1 j}^{(1)} \\ G_{i_2 j}^{(1)} \\ G_{i_3 j}^{(1)} \\ \vdots \\ G_{i_{(N_z N_y)} j}^{(1)} \end{pmatrix} + \begin{pmatrix} G_{i_1 k_{(N_y^p+1)}}^{(1)} V_{k_{(N_y^p+1)}} & G_{i_1 k_{(N_y^p+2)}}^{(1)} V_{k_{(N_y^p+2)}} & \cdots & G_{i_1 k_{(2N_y^p)}}^{(1)} V_{k_{(2N_y^p)}} \\ G_{i_2 k_{(N_y^p+1)}}^{(1)} V_{k_{(N_y^p+1)}} & G_{i_2 k_{(N_y^p+2)}}^{(1)} V_{k_{(N_y^p+2)}} & \cdots & G_{i_2 k_{(2N_y^p)}}^{(1)} V_{k_{(2N_y^p)}} \\ G_{i_3 k_{(N_y^p+1)}}^{(1)} V_{k_{(N_y^p+1)}} & G_{i_3 k_{(N_y^p+2)}}^{(1)} V_{k_{(N_y^p+2)}} & \cdots & G_{i_3 k_{(2N_y^p)}}^{(1)} V_{k_{(2N_y^p)}} \\ \vdots & \vdots & \vdots & \vdots \\ G_{i_{(N_z N_y)} k_{(N_y^p+1)}}^{(1)} V_{k_{(N_y^p+1)}} & G_{i_{(N_z N_y)} k_{(N_y^p+2)}}^{(1)} V_{k_{(N_y^p+2)}} & \cdots & G_{i_{(N_z N_y)} k_{(2N_y^p)}}^{(1)} V_{k_{(2N_y^p)}} \end{pmatrix} \begin{pmatrix} \Delta_{area} G_{k_{(N_y^p+1)j}}^{(2)} \\ \Delta_{area} G_{k_{(N_y^p+2)j}}^{(2)} \\ \Delta_{area} G_{k_{(N_y^p+3)j}}^{(2)} \\ \vdots \\ \Delta_{area} G_{k_{(2N_y^p)j}}^{(2)} \end{pmatrix} \quad (17)$$

• *Sub-step 4:* Before moving onto the next main iteration step (main iteration step number 3), the following sub-step evaluations has to be performed to estimate $[G_{k_{(N_y^p+1 \rightarrow 2N_y^p)k_{(2N_y^p+1 \rightarrow N_y^p N_z^p)}}}^{(2)}]$ and $[G_{ik_{(2N_y^p+1 \rightarrow N_y^p N_z^p)}}^{(2)}]$ to be used

in the next main iteration step. Here $(2N_y^P + 1 \rightarrow N_y^P N_z^P)$ corresponds to the remaining scatter position where the perturbation is brought-in in the future iteration steps by introducing slice number 3,4,5 etc..

Using Eq. 16,

$$\left[G_{k_{(N_y^P+1 \rightarrow 2N_y^P), k_{(2N_y^P+1 \rightarrow N_y^P N_z^P)}}^{(2)}} \right] = \left[I - \left[M_{(N_y^P+1 \rightarrow 2N_y^P)}^{(1)} \right] \right]^{-1} \left[G_{k_{(N_y^P+1 \rightarrow 2N_y^P), k_{(2N_y^P+1 \rightarrow N_y^P N_z^P)}}^{(1)}} \right] \quad (18)$$

Taking Eq. 17 and substituting for j as $k_{(2N_y^P+1 \rightarrow N_y^P N_z^P)}$, together with the above given equation, $[G_{ik_{(2N_y^P+1 \rightarrow N_y^P N_z^P)}}^{(2)}]$ can be estimated. The estimated $[G_{ik_{(2N_y^P+1 \rightarrow N_y^P N_z^P)}}^{(2)}]$ can be overwritten upon the existing memory taken by $G_{ik}^{(1)}$. Following the same logic, the main step 3 involving the slice of scatterers denoted by $2N_y^P + 1 \rightarrow 3N_y^P$ can be evaluated. The iteration process continues until the last slice of scatterers are brought in, obtaining the fully perturbed Green's function G_{ij} .

III. HOMOGENEOUS BOUNDARY CONDITIONS SATISFIED BY THE GREEN'S FUNCTION AND THE EIGENMODES

$$G(r, r_0)|_{z < z_0, (z, y) \in \Gamma_L} = \sum_{m=1}^{\infty} G_m(z, y, z_0, y_0)|_{z < z_0, (z, y) \in \Gamma_L} = \sum_{m=1}^{\infty} \underbrace{g_m^-(z_0, y_0) \psi_m^-(z, y)}_{G_m(z, y, z_0, y_0)|_{z < z_0, (z, y) \in \Gamma_L}}|_{z < z_0, (z, y) \in \Gamma_L} \quad (19)$$

$$G(r, r_0)|_{z \geq z_0, (z, y) \in \Gamma_R} = \sum_{m=1}^{\infty} G_m(z, y, z_0, y_0)|_{z \geq z_0, (z, y) \in \Gamma_R} = \sum_{m=1}^{\infty} \underbrace{g_m^+(z_0, y_0) \psi_m^+(z, y)}_{G_m(z, y, z_0, y_0)|_{z \geq z_0, (z, y) \in \Gamma_R}}|_{z \geq z_0, (z, y) \in \Gamma_R} \quad (20)$$

Both the propagating and the evanescent eigenmodes satisfy the following homogeneous boundary condition at the boundaries Γ_L and Γ_R ,

$$\frac{\partial}{\partial z} \psi_m^\pm(z, y) \mp ik_z^m \psi_m^\pm(z, y) = 0, \quad (21)$$

where in particular $k_z^{(m)} = ik_{z, ev}^{(m)}$ for the evanescent eigenmodes. As the disorder perturbation doesn't change the boundary conditions of eigenmodes associated with the outgoing Green's function waves, the following homogeneous boundary condition can be formed in terms of $G_m(z, y, z_0, y_0)$ similar to that of Eq. 21.

$$\left\{ \frac{\partial}{\partial z} G_m(r, r_0) + ik_z^{(m)} G_m(r, r_0) \right\} |_{z < z_0, (z, y) \in \Gamma_L} = 0 \quad (22)$$

$$\left\{ \frac{\partial}{\partial z} G_m(r, r_0) - ik_z^{(m)} G_m(r, r_0) \right\} |_{z \geq z_0, (z, y) \in \Gamma_R} = 0 \quad (23)$$

IV. SIMPLIFYING KIRCHHOFF–HELMHOLTZ BOUNDARY INTEGRAL EQUATION

As there is no flux flowing out of the transverse boundaries Γ_U and Γ_D , the boundary integral equation Eq. 13 can be simplified as

$$\int \left\{ \tilde{E}(r) \frac{\partial}{\partial z} G(r, r_0) \hat{e}_z - G(r, r_0) \frac{\partial}{\partial z} \tilde{E}(r) \hat{e}_z \right\} |_{(z, y) \in \Gamma_L} \cdot (-\hat{e}_z) dy + \int \left[\tilde{E}(r) \frac{\partial}{\partial z} G(r, r_0) \hat{e}_z - G(r, r_0) \frac{\partial}{\partial z} \tilde{E}(z, y) \hat{e}_z \right] |_{(z, y) \in \Gamma_R} \cdot \hat{e}_z dy = \tilde{E}(z_0, y_0) |_{(z_0, y_0) \in \Omega} \quad (24)$$

There is a minus sign associated with the $-\hat{e}_z dy$ on the first integral of the L.H.S in Eq. 24. This is due to the sign convention that the surface normal \hat{n} points outwards on Γ_L which is in opposite direction to $\hat{e}_z \frac{\partial}{\partial z}$ terms. The boundary integral equation Eq. 24, can be further simplified as both $G(z, z, y, y_0)$ and the total field $\tilde{E}(z, y, z_0, y_0)|_{(z,y) \in \Gamma_L \text{ or } (z,y) \in \Gamma_R}$ can be expanded in terms of eigenmodes $\psi_m^\pm(z, y)|_{(z,y) \in \Gamma_L, \Gamma_R}$ followed by the use of associated boundary conditions to be explained as the following. Let the wave incidence be from the left side of the disorder onto Γ_L . The total wave on Γ_L is the sum of incident wave modes and reflected wave modes. As the $E(z, y)$ in Eq. 24 is the total field, the first step to simplify is to provide explicit expression for $\tilde{E}(z, y)$ close to the boundary Γ_L and Γ_R followed by the use boundary conditions involving z derivatives of $\tilde{E}(z, y)$ and $G(z, y, z_0, y_0)$ to be explained in the following section. For $(z, y) \in \Gamma_L$,

$$\tilde{E}(z, y) = \tilde{E}^{inc}(z, y) + \tilde{E}^{refl}(z, y), \quad (25)$$

$$\text{where } \tilde{E}^{inc}(z, y)|_{(z,y) \in \Gamma_L} = \sum_{m=1}^{M_{total}} c_m^+ \chi_m(y) \phi_m^+(z) \quad (26)$$

$$\text{such that } \phi_m^+(z) = \begin{cases} \phi_{m,pr}^+(z) & \text{when } m \leq M_{pr} \\ \phi_{m,ev}^+(z, z_L) & \text{when } m > M_{pr} \end{cases} \quad \text{and}$$

$$\tilde{E}^{refl}(z, y)|_{(z,y) \in \Gamma_L} = \sum_{n=1}^{N_{total}} r_n^- \chi_n(y) \phi_n^-(z) \text{ such that } \phi_n^-(z) = \begin{cases} \phi_{n,pr}^-(z) & \text{when } n \leq N_{pr} \\ \phi_{n,ev}^-(z, z_L) & \text{when } n > N_{pr} \end{cases} \quad (27)$$

$$\text{and } r_n^- = \sum_{m=1}^{M_{total}} S_{11}^{nm} c_m^+ \quad (28)$$

Here, r_n^- is the reflection coefficient. Substituting equations Eq. 26 and Eq. 27 in Eq. 25, and using the property of the Kronecker delta function, the following is obtained.

$$\tilde{E}(z, y)|_{(z,y) \in \Gamma_L} = \sum_{n=1}^{N_{total}} \sum_{m=1}^{M_{total}} c_m^+ \phi_m^+(z) \chi_m(y) \delta_{kron}(n, m)|_{(z,y) \in \Gamma_L} + \sum_{n=1}^{N_{total}} \sum_{m=1}^{M_{total}} c_m^+ S_{11}^{nm} \chi_n(y) \phi_n^-(z)|_{(z,y) \in \Gamma_L} \quad (29)$$

Due to the Kronecker delta on the first term on the R.H.S of the above given equation, the index m can be replaced by n to obtain

$$\tilde{E}(z, y)|_{(z,y) \in \Gamma_L} = \sum_{n=1}^{N_{total}} \underbrace{\sum_{m=1}^{M_{total}} c_m^+ \{ \phi_n^+(z) \chi_n(y) \delta_{kron}(n, m) + S_{11}^{nm} \chi_n(y) \phi_n^-(z) \}}_{\tilde{E}_n(z, y)|_{(z,y) \in \Gamma_L}} = \sum_{n=1}^{N_{total}} \tilde{E}_n(z, y)|_{(z,y) \in \Gamma_L} \quad (30)$$

Eq. 30 denotes that the total field on Γ_L can be written as a series summation involving $\tilde{E}_n(z, y)|_{(z,y) \in \Gamma_L}$ waves. Next, the boundary condition associated with $\tilde{E}_n(z, y)|_{(z,y) \in \Gamma_L}$ waves for simplifying the boundary integral equation is provided.

$$\frac{\partial}{\partial z} \tilde{E}_n(z, y)|_{(z,y) \in \Gamma_L} + ik_z^{(n)} \tilde{E}_n(z, y)|_{(z,y) \in \Gamma_L} = \begin{cases} 2ik_z^{(n)} \tilde{E}_n^{inc}(z, y)|_{(z,y) \in \Gamma_L}, & \text{if } 1 \leq n \leq M_{total} \\ 0, & \text{if } n > M_{total} \end{cases} \quad (31)$$

where $\tilde{E}_n^{inc}(z, y)|_{(z,y) \in \Gamma_L} = c_n^+ \psi_n^+(z, y)|_{(z,y) \in \Gamma_L}$ is the n^{th} eigenmode term associated with the incident wave incident on the disorder from the left and $k_z^{(n)} = ik_{z,ev}^{(n)}$ for evanescent waves. Next is to evaluate the transmitted total field on Γ_R due to the wave incidence from the left side upon Γ_L and the associated boundary condition.

$$\tilde{E}(z, y)|_{(z,y) \in \Gamma_R} = \tilde{E}^{trans}(z, y)|_{(z,y) \in \Gamma_R} = \sum_{n=1}^{N_{total}} t_n^+ \phi_n^+(z) \chi_n(y)|_{(z,y) \in \Gamma_R} \quad (32)$$

$$\text{such that } \phi_n^+(z) = \begin{cases} \phi_{n,pr}^+(z) & \text{when } n \leq N_{pr} \\ \phi_{n,ev}^+(z, z_R) & \text{when } n > N_{pr} \end{cases}$$

where the field transmission coefficient term t_n^+ is related to the transmission matrix S_{21} by

$$t_n^+ = \sum_{m=1}^{M_{total}} S_{21}^{nm} c_m^+ \quad (33)$$

Therefore,

$$\tilde{E}(z, y)|_{(z,y) \in \Gamma_R} = \sum_{n=1}^{N_{total}} \underbrace{\left\{ \sum_{m=1}^{M_{total}} c_m^+ S_{21}^{nm} \right\}}_{\tilde{E}_n(z, y)|_{(z,y) \in \Gamma_R}} \phi_n^+(z) \chi_n(y) |_{(z,y) \in \Gamma_R} \quad (34)$$

$$= \sum_{n=1}^{N_{total}} \tilde{E}_n(z, y)|_{(z,y) \in \Gamma_R} \quad (35)$$

Similar to that of Eq. 31, one could form a boundary condition for $E_n(z, y)|_{(z,y) \in \Gamma_R}$ on the right boundary Γ_R as given below, to be used to simplify the boundary integral equation given in Eq. 24. This homogeneous boundary condition can be easily verified using equations Eq. 34 and Eq. 35.

$$\frac{\partial}{\partial z} \tilde{E}_n(z, y)|_{(z,y) \in \Gamma_R} - ik_z^{(n)} \tilde{E}_n(z, y)|_{(z,y) \in \Gamma_R} = 0 \quad (36)$$

A key aspect of simplifying Eq. 24 is to substitute the basis expansion for $G(z, z_0, y, y_0) = \sum_{m=1}^{M_{total}} G_m(z, y, z_0, y_0)$ and $\tilde{E}(z, y)|_{(z,y) \in \Gamma_{L/R}} = \sum_{n=1}^{N_{total}} \tilde{E}_n(z, y)|_{(z,y) \in \Gamma_{L/R}}$ and their corresponding boundary conditions while simplifying.

$$\begin{aligned} & \int \left\{ \sum_n \tilde{E}_n(z, y) \frac{\partial}{\partial z} \sum_m G_m(z, y, z_0, y_0) \hat{e}_z - \sum_m G_m(z, y, z_0, y_0) \frac{\partial}{\partial z} \sum_n \tilde{E}_n(z, y) \hat{e}_z \right\} |_{(z,y) \in \Gamma_L} \cdot (-\hat{e}_z) dy + \\ & \int \left\{ \sum_n \tilde{E}_n(z, y) \frac{\partial}{\partial z} \sum_m G_m(z, y, z_0, y_0) \hat{e}_z - \sum_m G_m(z, y, z_0, y_0) \frac{\partial}{\partial z} \sum_n \tilde{E}_n(z, y) \hat{e}_z \right\} |_{(z,y) \in \Gamma_R} \cdot \hat{e}_z dy \\ & = \tilde{E}(z_0, y_0) |_{(z_0, y_0) \in \Omega} \end{aligned} \quad (37)$$

As there is a $\chi_m(y)$ in $G_m(z, y, z_0, y_0)$ and a $\chi_n(y)$ in $\tilde{E}_n(z, y)$, due to orthogonality relation that $\int \chi_m(y) \chi_n(y) dy = \delta_{kron}(m, n)$, y integral of all the cross product terms where $m \neq n$, is zero. Hence only the terms $m = n$ remains non-zero. Therefore,

$$\begin{aligned} & \int \sum_n \left\{ \tilde{E}_n(z, y) \frac{\partial}{\partial z} G_n(z, y, z_0, y_0) \hat{e}_z - G_n(z, y, z_0, y_0) \frac{\partial}{\partial z} \tilde{E}_n(z, y) \hat{e}_z \right\} |_{(z,y) \in \Gamma_L} \cdot (-\hat{e}_z) dy + \\ & \int \sum_n \left\{ \tilde{E}_n(z, y) \frac{\partial}{\partial z} G_n(z, y, z_0, y_0) \hat{e}_z - G_n(z, y, z_0, y_0) \frac{\partial}{\partial z} \tilde{E}_n(z, y) \hat{e}_z \right\} |_{(z,y) \in \Gamma_R} \cdot \hat{e}_z dy = \tilde{E}(z_0, y_0) |_{(z_0, y_0) \in \Omega} \end{aligned} \quad (38)$$

Substituting the previously obtained boundary conditions (equations Eq. 23, Eq. 36, Eq. 22 and Eq. 31) in the above given form of boundary integral, the following simplified expression is obtained after some simple calculations.

$$\int \sum_n 2ik_z^{(n)} \tilde{E}_n^{inc}(z, y) G_n(z, y, z_0, y_0) |_{(z,y) \in \Gamma_L} dy = \tilde{E}(z_0, y_0) |_{(z_0, y_0) \in \Omega} \quad (39)$$

One could safely add a summation \sum_m to the $G_m(z, y, z_0, y_0)$ term in the above equation due to the orthogonality relationship $\int \chi_m(y) \chi_n(y) dy = \delta_{kron}(m, n)$. Therefore, the meaning of the integral given in Eq. 39 doesn't change if it is written in the following form

$$\int \sum_n 2ik_z^{(n)} \tilde{E}_n^{inc}(z, y) \sum_m G_m(z, y, z_0, y_0) |_{(z,y) \in \Gamma_L} dy = \tilde{E}(z_0, y_0) |_{(z_0, y_0) \in \Omega} \quad (40)$$

Replacing the expression for $\sum_m G_m(z, y, z_0, y_0)$ as $G(z, y, z_0, y_0)$ and changing the index n to m , the boundary integral takes a simpler form as given below. For wave incidence only from the left to right of the disorder (incidence onto Γ_L),

$$\sum_{m=1}^{M_{total}} 2ik_z^{(m)} \int \tilde{E}_m^{inc}(z, y) G(z, y, z_0, y_0) |_{(z,y) \in \Gamma_L} dy = \tilde{E}(z_0, y_0) |_{(z_0, y_0) \in \Omega} \quad (41)$$

where $\tilde{E}_m^{inc}(z, y)|_{(z,y) \in \Gamma_L} = c_m^+ \psi_m^+(z, y)|_{(z,y) \in \Gamma_L}$, $k_z^{(m)} = ik_{z, ev}^{(m)}$ when $m > M_{pr}$ and $M_{total} = M_{pr} + M_{ev}$, the total number of eigenmodes considered.

V. DERIVATION OF GENERALIZED FISHER-LEE RELATIONSHIPS

Generalized Fisher-Lee relations are obtained by substituting expression for the total field $\tilde{E}(z_0, y_0)$ in the boundary integral equation and solving for the reflection or transmission coefficients.

A. Derivation for S_{11}

First, let the wave incidence be from the left side of the disorder onto Γ_L . For estimating the reflection matrix S_{11} need to take $(z_0, y_0) \in \Gamma_L$. Then, the simplified boundary integral equation becomes,

$$\begin{aligned} & \sum_{m=1}^{M_{total}} 2ik_z^{(m)} \int \tilde{E}_m^{inc}(z, y) G(z, y, z_0, y_0) dy |_{(z,y) \in \Gamma_L \& (z_0, y_0) \in \Gamma_L} = \tilde{E}(z_0, y_0) |_{(z_0, y_0) \in \Gamma_L} = \sum_{n=1}^{N_{total}} \tilde{E}_n(z_0, y_0) |_{(z_0, y_0) \in \Gamma_L} \\ & = \sum_{m=1}^{M_{total}} \sum_{n=1}^{N_{total}} c_m^+ [\delta_{kron}(n, m) \chi_n(y_0) \phi_n^+(z_0) + S_{11}^{nm} \chi_n(y_0) \phi_n^-(z_0)] |_{(z_0, y_0) \in \Gamma_L} \end{aligned} \quad (42)$$

Comparing the summation terms covered by $\sum_{m=1}^{M_{total}}$ on *L.H.S* and *R.H.S*,

$$\begin{aligned} & 2ik_z^{(m)} c_m^+ \phi_m^+(z) \int \chi_m(y) G(z, y, z_0, y_0) dy |_{(z,y) \in \Gamma_L \& (z_0, y_0) \in \Gamma_L} = \\ & \sum_{n=1}^{N_{total}} c_m^+ [\delta_{kron}(n, m) \phi_n^+(z_0) \chi_n(y_0) + S_{11}^{nm} \chi_n(y_0) \phi_n^-(z_0)] |_{(z_0, y_0) \in \Gamma_L} \end{aligned} \quad (43)$$

Using the orthogonality relationship involving $\chi_n'(y)$ and integrating with respect to y_0 on both sides of the above given equation,

$$\begin{aligned} & 2ik_z^{(m)} \phi_m^+(z) c_m^+ \int_{y_0} \int_y \chi_m(y) G(z, y, z_0, y_0) \chi_{n'}(y_0) dy dy_0 |_{(z,y) \in \Gamma_L \& (z_0, y_0) \in \Gamma_L} = \\ & \int_{y_0} \chi_{n'}(y_0) \left\{ \sum_{n=1}^{N_{total}} c_m^+ [\delta_{kron}(n, m) \phi_n^+(z_0) \chi_n(y_0) + S_{11}^{nm} \chi_n(y_0) \phi_n^-(z_0)] dy_0 \right\} |_{(z_0, y_0) \in \Gamma_L} \\ & = c_m^+ \left\{ \delta_{kron}(n', m) \phi_{n'}^+(z_0) + S_{11}^{mn'} \phi_{n'}^-(z_0) \right\} \end{aligned} \quad (44)$$

On comparing the coefficients of c_m^+ on *L.H.S* and *R.H.S* of the previous equation,

$$2ik_z^{(m)} \phi_m^+(z) \int_{y_0} \int_y \chi_m(y) G(z, y, z_0, y_0) \chi_{n'}(y_0) |_{(z,y) \in \Gamma_L \& (z_0, y_0) \in \Gamma_L} dy dy_0 = \delta_{kron}(n', m) \phi_{n'}^+(z_0) + S_{11}^{mn'} \phi_{n'}^-(z_0) \quad (45)$$

Simplification : Rename n' as n and let z and z_0 be positioned at 0 on the left boundary. Therefore,

$$\begin{aligned} & 2ik_z^{(m)} \phi_m^+(z=0) \int_{y_0} \int_y \chi_m(y) G(z=0, y, z_0=0, y_0) \chi_n(y_0) |_{(z=0,y) \in \Gamma_L \& (z_0=0,y_0) \in \Gamma_L} dy dy_0 = \\ & \delta_{kron}(n, m) \phi_n^+(z_0=0) + S_{11}^{nm} \phi_n^-(z_0=0) \end{aligned} \quad (46)$$

Mathematically, there are 4 different possibilities with respect to the nature of incident and reflected modes.

Case 1 : Both input and output modes are propagating $m \leq M_{prop}$ and $n \leq N_{prop}$

$$2ik_z^{(m)} \frac{1}{\sqrt{k_z^{(m)}}} \int_{y_0} \int_y \chi_m(y) G(z, y, z_0, y_0) \chi_n(y_0) |_{(z=0,y) \in \Gamma_L \& (z_0=0,y_0) \in \Gamma_L} dy dy_0 = \delta_{kron}(n, m) \frac{1}{\sqrt{k_z^{(n)}}} + \frac{S_{11}^{nm}}{\sqrt{k_z^{(n)}}} \quad (47)$$

Case 2 : Input mode and output modes are evanescent $m > M_{prop}$ and $n > N_{prop}$

$$2ik_z^{(m)} \frac{1}{\sqrt{|k_z^{(m)}|}} \int_{y_0} \int_y \chi_m(y) G(z, y, z_0, y_0) \chi_n(y_0) |_{(z=0,y) \in \Gamma_L \& (z_0=0,y_0) \in \Gamma_L} dy dy_0 = \delta_{kron}(n, m) \frac{1}{\sqrt{|k_z^{(n)}|}} + S_{11}^{nm} \frac{1}{\sqrt{|k_z^{(n)}|}} \quad (48)$$

Case 3 : Input modes are propagating and output modes are evanescent $m \leq M_{prop}$ and $n > N_{prop}$

$$2ik_z^{(m)} \frac{1}{\sqrt{k_z^{(m)}}} \int_{y_0} \int_y \chi_m(y) G(z, y, z_0, y_0) \chi_n(y_0) |_{(z=0, y) \in \Gamma_L \& (z_0=0, y_0) \in \Gamma_L} dy dy_0 = \delta_{kron}(n, m) \frac{1}{\sqrt{k_z^{(n)}}} + S_{11}^{nm} \frac{1}{\sqrt{|k_z^{(n)}|}} \quad (49)$$

But $\delta_{kron}(n, m) = 0$, if $m \leq M_{prop}$ and $n > N_{prop}$

Case 4 : Input modes are evanescent and output modes are propagating $m > M_{prop}$ and $n \leq N_{prop}$

$$2ik_z^{(m)} \frac{1}{\sqrt{|k_z^{(m)}|}} \int_{y_0} \int_y \chi_m(y) G(z, y, z_0, y_0) \chi_n(y_0) |_{(z=0, y) \in \Gamma_L \& (z_0=0, y_0) \in \Gamma_L} dy dy_0 = \delta_{kron}(n, m) \frac{1}{\sqrt{|k_z^{(n)}|}} + S_{11}^{mn} \frac{1}{\sqrt{k_z^{(n)}}} \quad (50)$$

But $\delta_{kron}(n, m) = 0$, if $m > M_{prop}$ and $n \leq N_{prop}$.

Solving for S_{11} for cases 1, 2, 3 and 4, (using the information that for evanescent modes $\frac{k_z^{(m)}}{\sqrt{|k_z^{(m)}|}} = i\sqrt{|k_z^{(m)}|}$, is imaginary) are summarised in the Table I.

B. Derivation for S_{21}

Let the wave incidence be from the left side of the disorder onto Γ_L . For estimating the transmission matrix S_{21} , need to take $(z_0, y_0) \in \Gamma_R$. Then the simplified boundary integral equation becomes,

$$\begin{aligned} \sum_{m=1}^{M_{total}} 2ik_z^{(m)} \int \tilde{E}_m^{inc}(z, y) G(z, y, z_0, y_0) dy |_{(z, y) \in \Gamma_L \& (z_0, y_0) \in \Gamma_R} &= \tilde{E}(z_0, y_0) |_{(z_0, y_0) \in \Gamma_R} = \sum_{n=1}^{N_{total}} \tilde{E}_n(z_0, y_0) |_{(z_0, y_0) \in \Gamma_R} \\ &= \sum_{n=1}^{N_{total}} t_n^+ \chi_n(y_0) \phi_n^+(z_0) |_{(z_0, y_0) \in \Gamma_R} \\ &= \sum_{n=1}^{N_{total}} \left\{ \sum_{m=1}^{M_{total}} c_m^+ S_{21}^{nm} \right\} \chi_n(y_0) \phi_n^+(z_0) |_{(z_0, y_0) \in \Gamma_R} \quad (51) \end{aligned}$$

Comparing the summation terms covered by $\sum_{m=1}^{M_{total}}$ on *L.H.S* and *R.H.S*,

$$2ik_z^{(m)} \int c_m^+ \phi_m^+(z) \chi_m(y) G(z, y, z_0, y_0) dy |_{(z, y) \in \Gamma_L \& (z_0, y_0) \in \Gamma_R} = \sum_{n=1}^{N_{total}} c_m^+ S_{21}^{nm} \chi_n(y_0) \phi_n^+(z_0) |_{(z_0, y_0) \in \Gamma_R} \quad (52)$$

Using the orthogonality relationship involving $\chi_{n'}(y)$ and integrating with respect to y_0 on both sides of the above given equation,

$$2ik_z^{(m)} c_m^+ \phi_m^+(z) \int_y \int_{y_0} \chi_m(y) G(z, y, z_0, y_0) \chi_{n'}(y_0) dy dy_0 |_{(z, y) \in \Gamma_L \& (z_0, y_0) \in \Gamma_R} = c_m^+ S_{21}^{n'm} \phi_{n'}^+(z_0) |_{z_0 \in \Gamma_R} \quad (53)$$

On comparing the coefficients of c_m^+ on *L.H.S* and *R.H.S* of the previous equation,

$$2ik_z^{(m)} \phi_m^+(z) \int_y \int_{y_0} \chi_m(y) G(z, y, z_0, y_0) \chi_{n'}(y_0) dy dy_0 |_{(z, y) \in \Gamma_L \& (z_0, y_0) \in \Gamma_R} = S_{21}^{n'm} \phi_{n'}^+(z_0) |_{z_0 \in \Gamma_R} \quad (54)$$

Simplification : Rename n' as n and let z be positioned at 0 on the left boundary and $z_0 = z_R$ at Γ_R on the right boundary. Therefore,

$$\begin{aligned} 2ik_z^{(m)} \phi_m^+(z=0) \int_y \int_{y_0} \chi_m(y) G(z=0, y, z_0=z_R, y_0) \chi_n(y_0) dy dy_0 |_{(z=0, y) \in \Gamma_L \& (z_0=z_R, y_0) \in \Gamma_R} &= \\ S_{21}^{nm} \phi_n^+(z_0=z_R) |_{(z_0=z_R) \in \Gamma_R} & \quad (55) \end{aligned}$$

Mathematically, there are 4 different possibilities with respect to the nature of incident and transmitted modes.

Case 1 : Both input and output modes are propagating $m \leq M_{prop}$ and $n \leq N_{prop}$

$$2ik_z^{(m)} \frac{1}{\sqrt{k_z^{(m)}}} \int_y \int_{y_0} \chi_m(y) G(z, y, z_0, y_0) \chi_n(y_0) dy dy_0 |_{(z=0, y) \in \Gamma_L \& (z_0=z_R, y_0) \in \Gamma_R} = S_{21}^{nm} \frac{1}{\sqrt{k_z^{(n)}}} e^{+ik_z^{(n)} z_R} \quad (56)$$

Case 2 : Input mode and output modes are evanescent $m > M_{prop}$ and $n > N_{prop}$

$$2ik_z^{(m)} \frac{1}{\sqrt{|k_z^{(m)}|}} \int_y \int_{y_0} \chi_m(y) G(z, y, z_0, y_0) \chi_n(y_0) dy dy_0 |_{(z, y) \in \Gamma_L \& (z_0, y_0) \in \Gamma_R} = S_{21}^{nm} \frac{1}{\sqrt{|k_z^{(n)}|}} \quad (57)$$

Case 3 : Input modes are propagating and output modes are evanescent $m \leq M_{prop}$ and $n > N_{prop}$

$$2ik_z^{(m)} \frac{1}{\sqrt{k_z^{(m)}}} \int_y \int_{y_0} \chi_m(y) G(z, y, z_0, y_0) \chi_n(y_0) dy dy_0 |_{(z, y) \in \Gamma_L \& (z_0, y_0) \in \Gamma_R} = S_{21}^{nm} \frac{1}{\sqrt{|k_z^{(n)}|}} \quad (58)$$

Case 4 : Input modes are evanescent and output modes are propagating $m > M_{prop}$ and $n \leq N_{prop}$

$$2ik_z^{(m)} \frac{1}{\sqrt{|k_z^{(m)}|}} \int_y \int_{y_0} \chi_m(y) G(z, y, z_0, y_0) \chi_n(y_0) dy dy_0 |_{(z, y) \in \Gamma_L \& (z_0, y_0) \in \Gamma_R} = S_{21}^{nm} \frac{e^{+iz_R k_z^{(n)}}}{\sqrt{k_z^{(n)}}} \quad (59)$$

Solving for S_{21} for cases 1, 2, 3 and 4 (using the information that for evanescent modes $\frac{k_z^{(m)}}{\sqrt{|k_z^{(m)}|}} = i\sqrt{|k_z^{(m)}|}$, is imaginary) are summarised in the Table II.

C. Derivation for S_{22}

Let the wave incidence be from the right side of the disorder onto Γ_R . For estimating the reflection matrix S_{22} , need to take $(z_0, y_0) \in \Gamma_R$. Then the simplified boundary integral equation becomes,

$$\begin{aligned} & \sum_{m=1}^{M_{total}} 2ik_z^{(m)} \int E_m^{\text{inc}}(z, y) G(z, y, z_0, y_0) dy |_{(z, y) \in \Gamma_R \& (z_0, y_0) \in \Gamma_R} = \sum_{n=1}^{N_{total}} \tilde{E}_n(z_0, y_0) |_{(z_0, y_0) \in \Gamma_R} \\ & = \sum_{m=1}^{M_{total}} \sum_{n=1}^{N_{total}} c_m^- [\delta_{\text{kron}}(n, m) \phi_n^-(z_0) \chi_n(y_0) + S_{22}^{nm} \chi_n(y_0) \phi_n^+(z_0)] |_{(z_0, y_0) \in \Gamma_R} \end{aligned} \quad (60)$$

Performing the same set of operations as used for the derivation of S_{11} and setting $z = z_R$ and $z_0 = z_R$, the following is obtained

$$\begin{aligned} & 2ik_z^{(m)} \phi_m^-(z = z_R) \int_{y_0} \int_y \chi_m(y) G(z = z_R, y, z_0 = z_R, y_0) \chi_n(y_0) |_{(z=z_R, y) \in \Gamma_R \& (z_0=z_R, y_0) \in \Gamma_R} dy dy_0 = \\ & \{ \delta_{\text{kron}}(n, m) \phi_n^-(z_0 = z_R) + S_{22}^{nm} \phi_n^+(z_0 = z_R) \} |_{z_0=z_R \in \Gamma_R} \end{aligned} \quad (61)$$

Mathematically, there are 4 different possibilities with respect to the nature of incident and reflected modes.

Case 1 : Both input and output modes are propagating $m \leq M_{prop}$ and $n \leq N_{prop}$

$$\begin{aligned} & 2ik_z^{(m)} \frac{e^{-iz_R k_z^{(m)}}}{\sqrt{k_z^{(m)}}} \int_{y_0} \int_y \chi_m(y) G(z, y, z_0, y_0) \chi_n(y_0) |_{(z=z_R, y) \in \Gamma_R \& (z_0=z_R, y_0) \in \Gamma_R} dy dy_0 = \\ & \delta_{\text{kron}}(n, m) \frac{e^{-iz_R k_z^{(n)}}}{\sqrt{k_z^{(n)}}} + S_{22}^{nm} \frac{e^{+iz_R k_z^{(n)}}}{\sqrt{k_z^{(n)}}} \end{aligned} \quad (62)$$

Case 2 : Input mode and output modes are evanescent $m > M_{prop}$ and $n > N_{prop}$

$$2ik_z^{(m)} \frac{1}{\sqrt{|k_z^{(m)}|}} \int_{y_0} \int_y \chi_m(y) G(z, y, z_0, y_0) \chi_n(y_0) |_{(z=z_R, y) \in \Gamma_R \& (z_0=z_R, y_0) \in \Gamma_R} dy dy_0 =$$

$$\delta_{kron}(n, m) \frac{1}{\sqrt{|k_z^{(n)}|}} + S_{22}^{nm} \frac{1}{\sqrt{|k_z^{(n)}|}} \quad (63)$$

Case 3 : Input modes are propagating and output modes are evanescent $m \leq M_{prop}$ and $n > N_{prop}$

$$2ik_z^{(m)} \frac{e^{-iz_R k_z^{(m)}}}{\sqrt{k_z^{(m)}}} \int_{y_0} \int_y \chi_m(y) G(z, y, z_0, y_0) \chi_n(y_0) |_{(z, y) \in \Gamma_L \& (z_0, y_0) \in \Gamma_L} dy dy_0 =$$

$$\delta_{kron}(n, m) \frac{e^{-iz_R k_z^{(n)}}}{\sqrt{k_z^{(n)}}} + S_{22}^{nm} \frac{1}{\sqrt{|k_z^{(n)}|}} \quad (64)$$

But $\delta_{kron}(n, m) = 0$, if $m \leq M_{prop}$ and $n > N_{prop}$.

Case 4 : Input modes are evanescent and output modes are propagating $m > M_{prop}$ and $n \leq N_{prop}$

$$2ik_z^{(m)} \frac{1}{\sqrt{|k_z^{(m)}|}} \int_{y_0} \int_y \chi_m(y) G(z, y, z_0, y_0) \chi_n(y_0) |_{(z, y) \in \Gamma_L \& (z_0, y_0) \in \Gamma_L} dy dy_0 =$$

$$\delta_{kron}(n, m) \frac{1}{\sqrt{|k_z^{(n)}|}} + S_{22}^{nm} \frac{e^{+iz_R k_z^{(n)}}}{\sqrt{k_z^{(n)}}} \quad (65)$$

But $\delta_{kron}(n, m) = 0$, if $m > M_{prop}$ and $n \leq N_{prop}$.

Solving S_{22} for cases 1, 2, 3 and 4 (using the information that for evanescent modes $\frac{k_z^{(m)}}{\sqrt{|k_z^{(m)}|}} = i\sqrt{|k_z^{(m)}|}$, is imaginary) are summarised in the Table III.

D. Derivation for S_{12}

Let the wave incidence be from the right side of the disorder onto Γ_R . For estimating the transmission matrix S_{12} , need to take $(z_0, y_0) \in \Gamma_L$. Then the simplified boundary integral equation becomes,

$$\sum_{m=1}^{M_{total}} 2ik_z^{(m)} \int \tilde{E}_m^{inc}(z, y) G(z, y, z_0, y_0) dy |_{(z, y) \in \Gamma_R \& (z_0, y_0) \in \Gamma_L} = \sum_{n=1}^{N_{total}} \tilde{E}_n(z_0, y_0) |_{(z_0, y_0) \in \Gamma_L}$$

$$= \sum_{n=1}^{N_{total}} \left\{ \sum_{m=1}^{M_{total}} c_m^+ S_{12}^{nm} \right\} \chi_n(y_0) \phi_n^-(z_0) |_{(z_0, y_0) \in \Gamma_L} \quad (66)$$

Performing the same set of operations as used for the derivation of S_{21} and setting $z = z_R$ and $z_0 = z_L$, the following is obtained

$$2ik_z^{(m)} \phi_m^-(z = z_R) \int_y \int_{y_0} \chi_m(y) G(z = z_R, y, z_0 = z_L, y_0) \chi_n(y_0) dy dy_0 |_{(z=z_R, y) \in \Gamma_R \& (z_0=z_L, y_0) \in \Gamma_L} =$$

$$S_{12}^{nm} \phi_{n'}^-(z_0) |_{(z_0=z_L) \in \Gamma_L} \quad (67)$$

Mathematically, there are 4 different possibilities with respect to the nature of incident and transmitted modes.

Case 1 : Both input and output modes are propagating $m \leq M_{prop}$ and $n \leq N_{prop}$

$$2ik_z^{(m)} \frac{e^{-iz_R k_z^{(m)}}}{\sqrt{k_z^{(m)}}} \int_y \int_{y_0} \chi_m(y) G(z, y, z_0, y_0) \chi_n(y_0) dy dy_0 |_{(z=z_R, y) \in \Gamma_R \& (z_0=z_L, y_0) \in \Gamma_L} = S_{12}^{nm} \frac{1}{\sqrt{k_z^{(n)}}} \quad (68)$$

Case 2 : Input mode and output modes are evanescent $m > M_{prop}$ and $n > N_{prop}$

$$2ik_z^{(m)} \frac{1}{\sqrt{|k_z^{(m)}|}} \int_y \int_{y_0} \chi_m(y) G(z, y, z_0, y_0) \chi_n(y_0) dy dy_0 |_{(z=z_R, y) \in \Gamma_R \& (z_0=z_L, y_0) \in \Gamma_L} = S_{12}^{nm} \frac{1}{\sqrt{|k_z^{(n)}|}} \quad (69)$$

Case 3 : Input modes are propagating and output modes are evanescent $m \leq M_{prop}$ and $n > N_{prop}$

$$2ik_z^{(m)} \frac{e^{-iz_R k_z^{(m)}}}{\sqrt{k_z^{(m)}}} \int_y \int_{y_0} \chi_m(y) G(z, y, z_0, y_0) \chi_n(y_0) dy dy_0 |_{(z=z_R, y) \in \Gamma_R \& (z_0=z_L, y_0) \in \Gamma_L} = S_{12}^{nm} \frac{1}{\sqrt{|k_z^{(n)}|}} \quad (70)$$

Case 4 : Input modes are evanescent and output modes are propagating $m > M_{prop}$ and $n \leq N_{prop}$

$$2ik_z^{(m)} \frac{1}{\sqrt{|k_z^{(m)}|}} \int_y \int_{y_0} \chi_m(y) G(z, y, z_0, y_0) \chi_n(y_0) dy dy_0 |_{(z, y) \in \Gamma_L \& (z_0, y_0) \in \Gamma_R} = \frac{S_{12}^{nm}}{\sqrt{k_z^{(n)}}} \quad (71)$$

Solving S_{12} for cases 1, 2, 3 and 4 (using the information that for evanescent modes $\frac{k_z^{(m)}}{\sqrt{|k_z^{(m)}|}} = i\sqrt{|k_z^{(m)}|}$, is imaginary) are summarized in the Table IV.

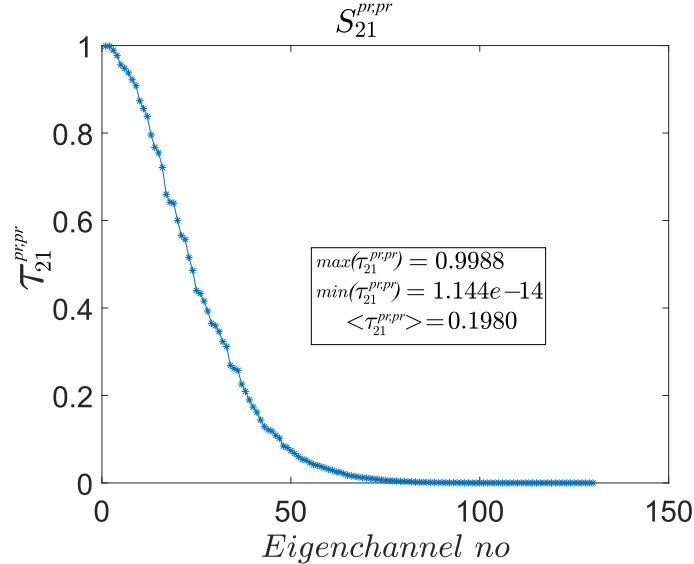


FIG. 1. **Eigenchannel transmission coefficients of $S_{21}^{pr,pr}$ are plotted for a disorder with the average eigenchannel transmission of 0.198.** Eigenchannel transmission coefficients contained in the diagonal of the matrix $\tau_{21}^{pr,pr}$, (obtained from the *S.V.D* of the $S_{21}^{pr,pr}$ matrix given in FIG. 2 of the main paper), is plotted. The maximum, minimum and average values of $\tau_{21}^{pr,pr}$ are also given. The averaging is done with respect to all the eigenchannels of the given disorder. Some of the corresponding eigenchannels are plotted in the supplementary FIG. 2.

VI. VISUALIZATION OF TRANSMISSION EIGENCHANNELS

For accessing the propagating eigenchannels, singular value decomposition (*S.V.D*) of the components of the $S^{pr,pr}$ matrix is performed. As an example, the propagating transmission eigenchannels for wave incidence only from the

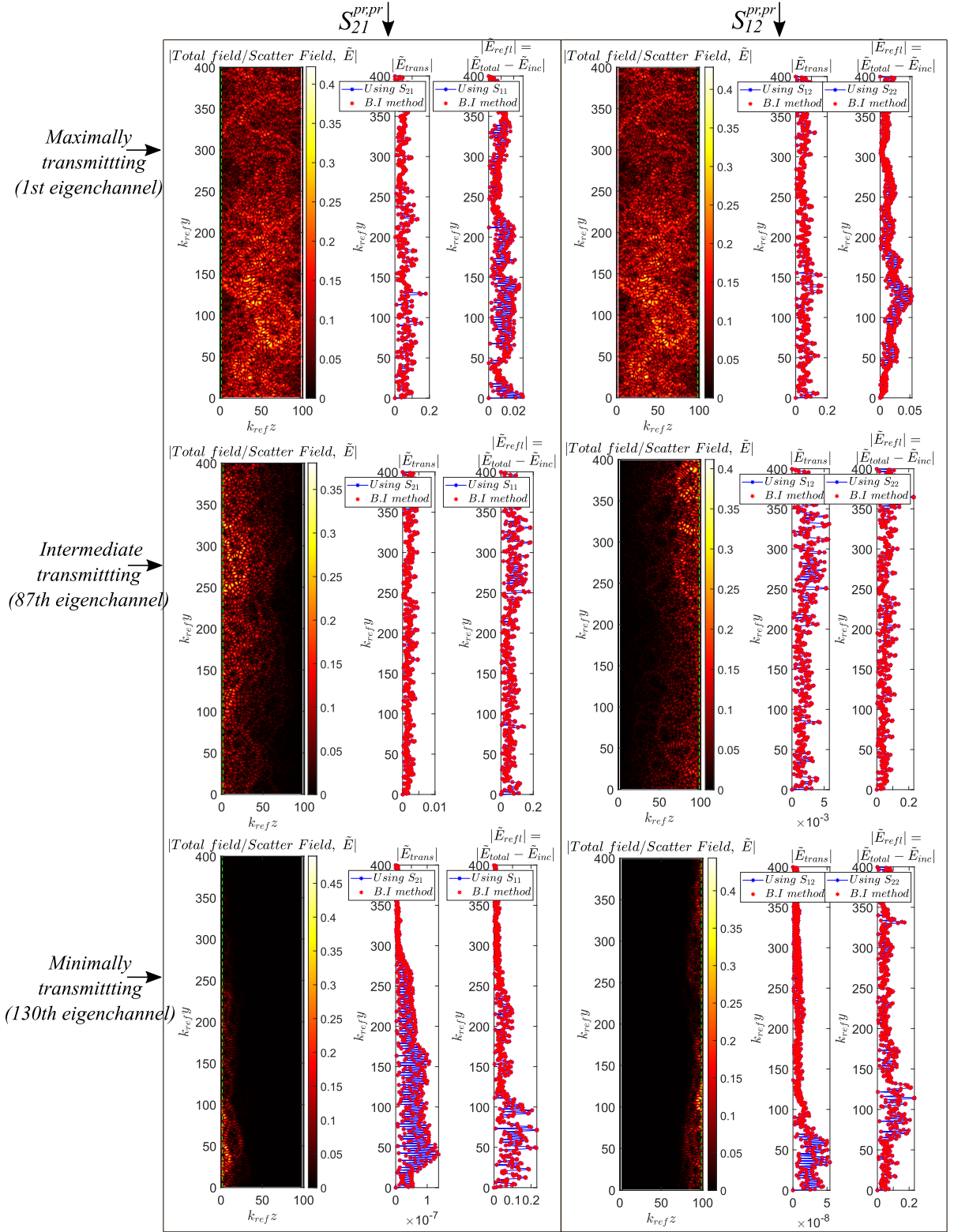


FIG. 2. Visualizing various eigenchannels of $S_{21}^{pr,pr}$ and $S_{12}^{pr,pr}$, containing 130 propagating eigenmodes and 30 evanescent eigenmodes, with $\langle \tau_{21}^{pr,pr} \rangle = 0.198$, the transmission averaged over various eigenchannels of the given disorder shown in FIG. 5 of the main paper. (a) Maximally transmitted (first) eigenchannel of $S_{21}^{pr,pr}$, where transmission, $T = 0.9988$ and reflection $R = 0.0012$ (b) An intermediate eigenchannel numbered 87 out of the 130 eigenchannel modes, of $S_{21}^{pr,pr}$, where $T = 0.0013$, $R = 0.9987$. (c) Minimally transmitted (last eigenchannel numbered 130) eigenchannel of $S_{21}^{pr,pr}$, where $T = 1.1438e - 14$, $R = 1$. Similarly, (d) Maximally transmitted (first) eigenchannel of $S_{12}^{pr,pr}$, where $T = 0.9988$, $R = 0.0012$ (e) An intermediate eigenchannel numbered 87 out of the 130 eigenchannel modes, of $S_{12}^{pr,pr}$, where $T = 0.0013$, $R = 0.9987$. (f) Minimally transmitted (last eigenchannel, numbered 130) eigenchannel of $S_{12}^{pr,pr}$, where $T = 1.1438e - 14$, $R = 1$. The transport paths associated with the maximally transmitted eigenchannel of $S_{21}^{pr,pr}$ and $S_{12}^{pr,pr}$ looks identical in the inside of the disorder. It is because the transport path taken from left to right with the maximum transmission close to unity, is the same path taken from right to left for maximal transmission.

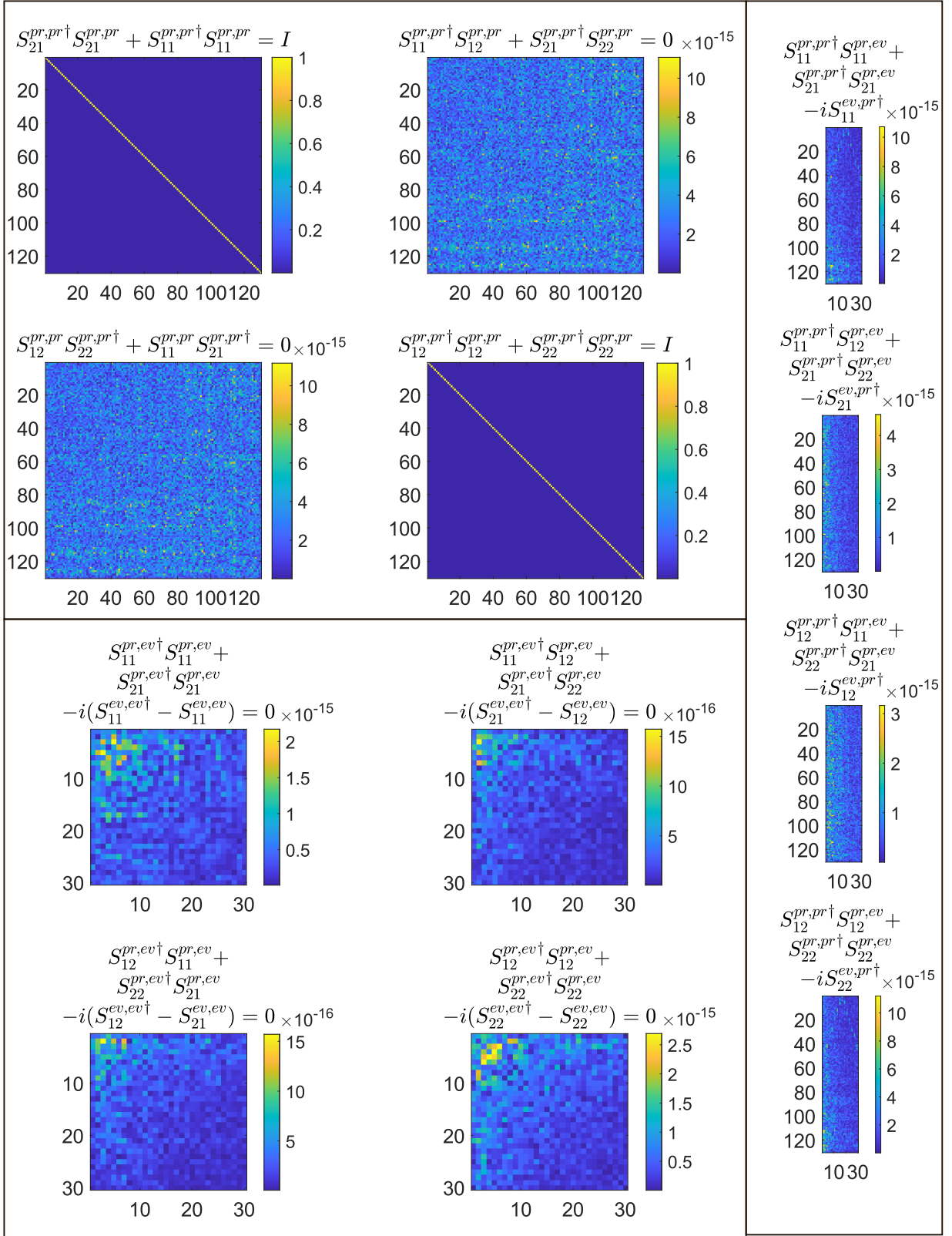


FIG. 3. **Additional numerical validation done for verifying the generalized unitarity relations.** For those unitarity relations where the R.H.S is a zero matrix analytically, the simulation code yields a numerical matrix close to be approximated to zero (of the order of 10^{-15}) as shown in the plots. For those unitarity relations where the R.H.S is a unit matrix analytically, the diagonal elements are all unity.

left-side of the disorder, is accessed by performing the *S.V.D* of $S_{21}^{pr,pr} = U_{21}\Sigma_{21}V_{21}^\dagger$ and using the first singular vector of V_{21} to maximize the transmission. $\tau_{21}^{pr,pr} = (\Sigma_{21}^{pr,pr})^2$ is the diagonal matrix containing the eigenchannels' transmission coefficients ranging from 0 to 1 as shown in the supplementary FIG. 1. For the disordered slab shown in FIG. 5 of the main paper, various eigenchannels, for the wave incidence from both the left side and the right side of the disorder, are shown in the supplementary FIG. 2.

VII. ADDITIONAL NUMERICAL VALIDATION OF THE GENERALIZED UNITARITY RELATION

In addition to the numerical validation of the compact form of the generalized unitarity relation given in the FIG. 3 of the main paper, additional validation is performed by decomposing the compact form into some of its individual components as given in the supplementary FIG. 3.

VIII. S MATRIX CASCADING AND ENSEMBLE AVERAGING

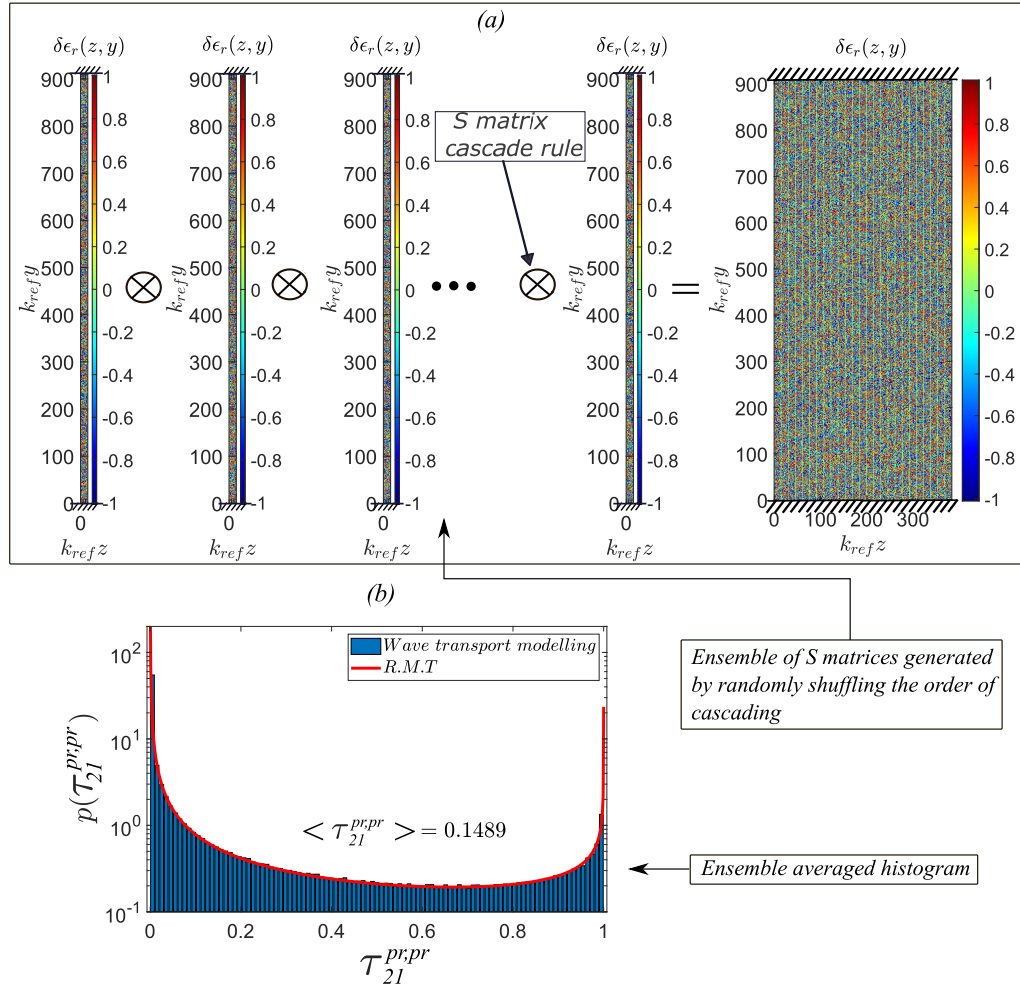


FIG. 4. **Schematic to demonstrate the *S* matrix cascade rule and the ensemble averaged eigenchannel transmission coefficient distribution obtained through cascading.** (a) Schematic of cascading thinner slabs to form thicker slab is shown. Cascade rule given in Eq. 74 is used to cascade the slabs. First, the first and the second thin slabs are cascaded. It is followed by cascading the third slab with the cascaded result obtained from the first and the second slab. This pattern is repeated, until the last thin slab is cascaded. (b) The ensemble averaged frequency distribution of $\tau_{21}^{pr,pr}$ values after cascading. It is compared with the bimodal distribution associated with the Random Matrix theory (*R.M.T*). Note that here the histogram is evaluated for individual cascaded disorders, followed by averaging the obtained histogram over many cascaded disorder realizations.

This section explains the S matrix cascading method by which, a larger disordered slab can be formed, by cascading an ensemble of thinner slabs. Cascading of the generalized S matrices of the thinner slabs, builds the sample along the longitudinal dimension (z axis) step-by-step, as shown in the schematic given in the supplementary FIG. 4(a). Different realizations of thicker slabs (1000 in number) can be formed from the same S matrices of the thinner slabs (25 in number), taken in random order. This is particularly advantageous from a computational point of view that, one need not model 1000 different large slabs, but could estimate the S matrices of a collection of smaller slabs once and cascade them using random order of the slabs for obtaining different realizations of larger slabs. The well known cascading formula for S matrices is given as the following.

$$S^{(a)} = \begin{pmatrix} S_{11}^{(a)} & S_{12}^{(a)} \\ S_{21}^{(a)} & S_{22}^{(a)} \end{pmatrix} \quad (72)$$

and

$$S^{(b)} = \begin{pmatrix} S_{11}^{(b)} & S_{12}^{(b)} \\ S_{21}^{(b)} & S_{22}^{(b)} \end{pmatrix} \quad (73)$$

$$\begin{aligned} S^{\text{cascade}} &= S^{(a)} \otimes S^{(b)} = \begin{pmatrix} S_{11}^{(a)} & S_{12}^{(a)} \\ S_{21}^{(a)} & S_{22}^{(a)} \end{pmatrix} \otimes \begin{pmatrix} S_{11}^{(b)} & S_{12}^{(b)} \\ S_{21}^{(b)} & S_{22}^{(b)} \end{pmatrix} \\ &= \begin{pmatrix} S_{11}^{(a)} + S_{12}^{(a)} \left(I - S_{11}^{(b)} S_{22}^{(a)} \right)^{-1} S_{11}^{(b)} S_{21}^{(a)} & S_{12}^{(a)} \left(I - S_{11}^{(b)} S_{22}^{(a)} \right)^{-1} S_{12}^{(b)} \\ S_{21}^{(b)} \left(I - S_{22}^{(a)} S_{11}^{(b)} \right)^{-1} S_{21}^{(a)} & S_{22}^{(b)} + S_{21}^{(b)} \left(I - S_{22}^{(a)} S_{11}^{(b)} \right)^{-1} S_{22}^{(a)} S_{12}^{(b)} \end{pmatrix} \end{aligned} \quad (74)$$

where I is the identity matrix. The S matrices for a collection of the smaller slabs, are estimated serially using the generalized Fisher-Lee relations, followed by the use of the cascading formula given in Eq. 74. This helps in the ensemble averaging of the focusing results in the main paper. The ensemble averaged eigenchannel transmission coefficients of $S_{21}^{pr,pr}$ after cascading is given in FIG. 4(b).